technologies

Review

Recent Technological Progress of Fiber-Optical Sensors for Bio-Mechatronics Applications

Mohomad Aqeel Abdhul Rahuman [1,†], Nipun Shantha Kahatapitiya [1,†], Viraj Niroshan Amarakoon [1], Udaya Wijenayake [2], Bhagya Nathali Silva [2], Mansik Jeon [3], Jeehyun Kim [3], Naresh Kumar Ravichandran [4,*] and Ruchire Eranga Wijesinghe [5,*]

1 Department of Materials and Mechanical Technology, Faculty of Technology, University of Sri Jayewardenepura, Pitipana, Homagama 10200, Sri Lanka; aqeelabdhulrahuman@gmail.com (M.A.A.R.); nipunshantha@gmail.com (N.S.K.); aavniroshan@gmail.com (V.N.A.)
2 Department of Computer Engineering, Faculty of Engineering, University of Sri Jayewardenepura, Nugegoda 10250, Sri Lanka; udayaw@sjp.ac.lk (U.W.); nathali.slv@sjp.ac.lk (B.N.S.)
3 School of Electronic and Electrical Engineering, College of IT Engineering, Kyungpook National University, 80, Daehak-ro, Buk-gu, Daegu 41566, Republic of Korea; msjeon@knu.ac.kr (M.J.); jeehk@knu.ac.kr (J.K.)
4 Center for Scientific Instrumentation, Korea Basic Science Institute, 169-148, Gwahak-ro, Yuseong-gu, Daejeon 34133, Republic of Korea
5 Department of Electrical and Electronic Engineering, Faculty of Engineering, Sri Lanka Institute of Information Technology, Malabe 10115, Sri Lanka
* Correspondence: nareshr9169@kbsi.re.kr (N.K.R.); eranga.w@sliit.lk (R.E.W.); Tel.: +94-74-153-1013 (R.E.W.)
† These authors contributed equally to this work and shared first authorship.

Abstract: Bio-mechatronics is an interdisciplinary scientific field that emphasizes the integration of biology and mechatronics to discover innovative solutions for numerous biomedical applications. The broad application spectrum of bio-mechatronics consists of minimally invasive surgeries, rehabilitation, development of prosthetics, and soft wearables to find engineering solutions for the human body. Fiber-optic-based sensors have recently become an indispensable part of bio-mechatronics systems, which are essential for position detection and control, monitoring measurements, compliance control, and various feedback applications. As a result, significant advancements have been introduced for designing and developing fiber-optic-based sensors in the past decade. This review discusses recent technological advancements in fiber-optical sensors, which have been potentially adapted for numerous bio-mechatronic applications. It also encompasses fundamental principles, different types of fiber-optical sensors based on recent development strategies, and characterizations of fiber Bragg gratings, optical fiber force myography, polymer optical fibers, optical tactile sensors, and Fabry–Perot interferometric applications. Hence, robust knowledge can be obtained regarding the technological enhancements in fiber-optical sensors for bio-mechatronics-based interdisciplinary developments. Therefore, this review offers a comprehensive exploration of recent technological advances in fiber-optical sensors for bio-mechatronics. It provides insights into their potential to revolutionize biomedical and bio-mechatronics applications, ultimately contributing to improved patient outcomes and healthcare innovation.

Keywords: bio-mechatronics; fiber-optical sensors; force myography; polymer optical fiber; optical tactile sensors; Fabry–Perot interferometry

Citation: Abdhul Rahuman, M.A.; Kahatapitiya, N.S.; Amarakoon, V.N.; Wijenayake, U.; Silva, B.N.; Jeon, M.; Kim, J.; Ravichandran, N.K.; Wijesinghe, R.E. Recent Technological Progress of Fiber-Optical Sensors for Bio-Mechatronics Applications. *Technologies* **2023**, *11*, 157. https://doi.org/10.3390/technologies11060157

Academic Editor: Manoj Gupta

Received: 25 September 2023
Revised: 14 October 2023
Accepted: 29 October 2023
Published: 7 November 2023

1. Introduction

The studies and research on bio-mechatronics and applications date back to the 1970s and 1980s as an effort to address the theoretical and experimental issues, especially those brought about by applications of mechatronics and robotics in the healthcare and medical domains [1]. One of the main goals of recently popular research into bio-mechatronic systems for technology and scientific exploration is to learn more about the mechanisms that drive biological systems. The current emphasis of bio-mechatronic research revolves around the applications and activities in humanoid and bioinspired robots [2], such as human–robot interaction [3], prostheses [4], endoscopic systems [5], minimally invasive surgeries (MISs) [6], physical parameter monitoring [7], health monitoring [8], and rehabilitation [9]. The measurement system that senses physiological parameter changes is one of the most crucial components of bio-mechatronic systems.

This measurement system typically consists of a sensor that detects changes in physiological parameters and a signal-conditioning circuit. Accurately measuring dynamic variables is crucial for the optimal operation of sensitive systems, such as bio-mechatronic systems. Until now, only clinical settings have been able to effectively use the accurate monitoring of physiological parameters since using sophisticated and complex technologies incurs high costs and requires skilled employees [10]. Innovative sensor technologies have recently been developed to deliver tools for bio-mechatronic systems that are non-invasive, affordable, and tailored to address these drawbacks [11,12].

Fiber optics play a significant role in the development of bio-mechatronic systems by providing non-invasive and accurate sensing capabilities. Optical fibers have unique properties, such as high sensitivity, low noise, and electromagnetic interference immunity, which make them ideal for monitoring physiological parameters in real time. These advantages make optical fibers an attractive alternative to traditional sensors for measuring a wide range of physiological signals.

In this account, the recent technological advancements of fiber-optical sensors (FOSs) for bio-mechatronic applications will be reviewed. An overview of various optical fiber sensors utilized in bio-mechatronics, operation principles, designs, and applications are discussed. The challenges faced by current FOSs and the strategies employed to overcome them will be examined. Additionally, the potential of FOSs to enhance the accuracy, reliability, and affordability of bio-mechatronic systems is highlighted. This review is divided into five main sections, which provide insights into various fiber-optic sensors and their use in bio-mechatronic applications, contributing to the overall understanding of advanced sensor technologies in the field. In Section 2, applications of fiber Bragg grating (FBG) technology are discussed along with the fundamental applications. Section 3 discusses the use of force myography (FMG) sensors in various applications, while Section 4 mentions the use of polymer optical fiber (POF) sensors in different applications. Section 5 discusses the use of optical tactile sensors. In Section 6, the advantages and applications of Fabry–Perot interferometry (FPI) fiber sensors are discussed. Finally, Section 7 outlines the potential advancements in bio-mechatronics through advanced fiber-optical sensors while addressing the limitations of fiber-optic sensors and emphasizing the need for further development. Table 1 provides all abbreviations and their full meanings used in this study.

Table 1. List of abbreviations.

Abbreviation	Definition
MIS	Minimally Invasive Surgery
FBG	Fiber Bragg Grating
SEM	Scanning Electron Microscopy
CPC	Calcium Phosphate Cement
CFRP	Carbon-Fiber-Reinforced Polymer
FMG	Force Myography
FSR	Force-Sensitive Resistor
PDMS	Polydimethylsiloxane
PLA	Polylactic Acid
EMG	Electro Myography
DAQ	Data Acquisition Device
PVC	Polyvinyl Chloride

Table 1. *Cont.*

Abbreviation	Definition
CCD	Charge-Coupled Device
MMF	Silica Multi-Mode Fiber
EDC	Extensor Digitorum Communis
FDP	Flexor Digitorum Profundus
AEP	Abductor/Extensor Pollicis
RMS	Root Mean Square
DNN	Deep Neural Network
FSR	Force-Sensing Resistor
POF	Polymer Optical Fiber
POF-SG	POF Strain Gauge
ALLOR	Advanced Lower-Limb Orthosis for Rehabilitation
ESG	Electronic Strain Gauge
GRF	Ground Reaction Force
PMMA	Polymethyl Methacrylate
3D	Three-Dimensional
RAMIS	Robot-Assisted Minimally Invasive Surgery
LED	Light-Emitting Diode
FEA	Finite Element Analysis
CBR	Constant Bending Radius
VBR	Variable Bending Radius
MAE	Mean Absolute Error
FPI	Fabry–Perot Interferometry
MRI	Magnetic Resonance Imaging
FP	Fabry–Perot
OCT	Optical Coherence Tomography
SMF	Single-Mode Fiber
TDM	time-division multiplexing
DOF	Degrees of Freedom
ANN	Artificial Neural Network

2. Fiber-Bragg-Grating-Based Instrumentation

At the forefront of optical sensing technologies, the FBG stands as a remarkable innovation. The FBG is a distributed Bragg reflector, which is formed by exposing the core of the fiber. Fiber Bragg grating sensors have gained considerable. Moreover, FBG sensor arrays can be fabricated by connecting multiple FBGs to different wavelengths in series along the length of a single fiber, which enables the acquisition of strain data at several points along the fiber. Recently, femtosecond laser technology was explored for fabricating microstructures, including FBGs [13]. It is worth noting that the biocompatibility and versatility of optical fiber sensors specifically refer to the capacity of FBG sensors to operate effectively in diverse biomedical applications, accommodating a broad range of strain levels. Optical fiber sensors incorporating FBGs have been widely used as strain sensors to measure various parameters and monitor prosthetics in biomedical engineering.

The refractive index within the core of an optical fiber is periodically modulated in the formation of FBGs (Figure 1). This is achieved through exposure to an intense optical interference pattern, creating a resonant structure that reflects a Bragg wavelength [14,15] while all the other wavelength components move through the FBG. The Bragg wavelength λB can be expressed as [16]

$$\lambda_B = 2\Lambda n_{eff}$$

where n_{eff} is the optical fiber's effective refractive index, and Λ is the grating period. When the grating is exposed to external disturbances, such as strain and temperature, a change occurs in the Bragg wavelength. Physical properties can be measured by precisely measuring this wavelength change [14]. The recent technological efforts to functionalize FBGs for minimally invasive surgery applications are discussed in Section 2.1.

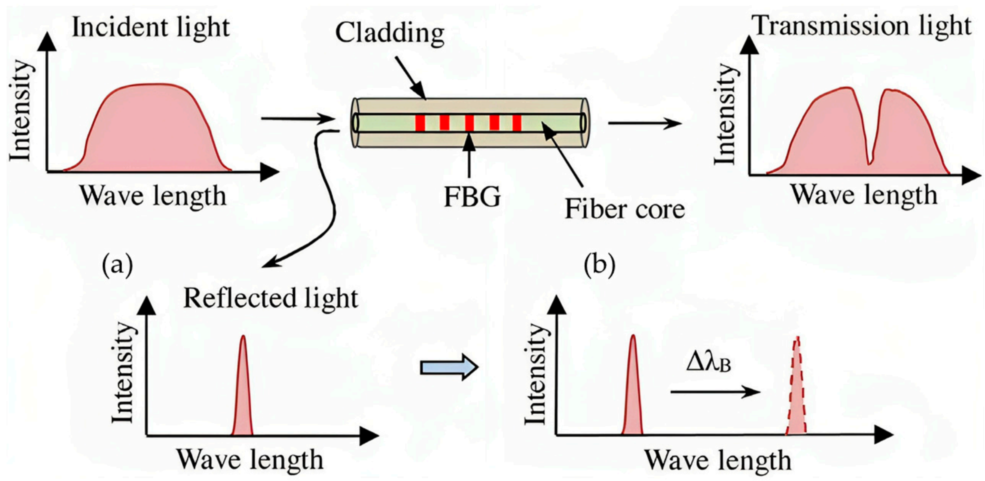

Figure 1. Fiber core and cladding of an FBG have distinct refractive indices. The FBG's exposure to external turbulences, such as strain and temperature, alters the Bragg wavelength, which will be back-reflected while other components of the wavelength will pass through the FBG. (**a**) The incident light is transmitted through the FBG, and a narrow band is back-reflected. (**b**) Shifted back-reflected band after applying external disturbances (adapted from [17]).

2.1. Minimally Invasive Surgeries (MISs)

MISs provide significant benefits for patients, such as reduced blood loss, less pain, faster recovery, and reduced infection rates. Thus, MIS has become a desirable alternative to conventional open surgeries in many surgical procedures [18,19]. Here, the surgeries are performed on organs by inserting specially designed instruments through small access points on the patient's skin into the body cavities and blood vessels [20]. However, emerging MIS systems have major limitations, such as the absence of force feedback during instrument–tissue interaction [20–23]. Therefore, surgeons solely rely on pseudo-haptic feedback [24] or visual force feedback [19] to perform the surgery. The precision and accuracy of the measured force are debatable in most cases because of internal friction in the tools and contact friction between the trocar and the tools. Undesired forces created by body cavities cause the forces perceived at the instrument to be greater than the actual force at the tip of the device [22,25].

Pouya Soltani Zarrin et al. developed a stainless-steel sterilizable grasper with two degrees of freedom (DOF) for a laparoscopic needle to sense grip and axial forces with high accuracy and resolution [22]. Its sensorized grasper consisted of two jaws, and each grasper jaw comprised deformable and fixed parts to increase axial sensitivity. A 3 mm FBG sensor was embedded into the lower jaw of the grasper. It was used to measure axial forces at the tip of the instrument, where embedding those sensors eliminates the effects of undesirable forces in the perceived axial force reading. For measuring grasping forces, an 8 mm FBG sensor was attached to the lower jaw with the help of glue. A force/torque sensor (F/T) was used to calibrate the axial and grasping sensors, and computer software was used to acquire and manipulate each sensor's information. Given the force stimuli, the grasping and axial FBG sensors show that 0.19 N (range, 0–10 N) and 0.26 N (range, 2–5 N) were the total root-mean-square (RMS) errors with the repeatability of 0.21 N and 0.35 N.

Moreover, Changhu LV et al. developed a palpation force sensor based on FBGs to inspect tissue abnormalities with high sensitivity and large sensing range in the course of robot-assisted minimally invasive surgery, as shown in Figure 2 [18].

The sensor incorporates two main components: a force-sensitive flexure based on the mechanism of sarrus linkage and a suspended optical fiber embedded with a 5 mm FBG element.

Figure 3a FBG interrogator with a sampling rate of 100 Hz and a wavelength resolution of 1 picometer (pm) was used to obtain the reflected wavelength that corresponds to the induced strain. In static force calibration, axial forces ranging from 0 to 5 N at 0.5 N intervals were applied, with corresponding FBG reflective wavelengths recorded. This process was repeated six times, and the average values during each loading step determined the force–wavelength relationship, shown in Figure 3b.

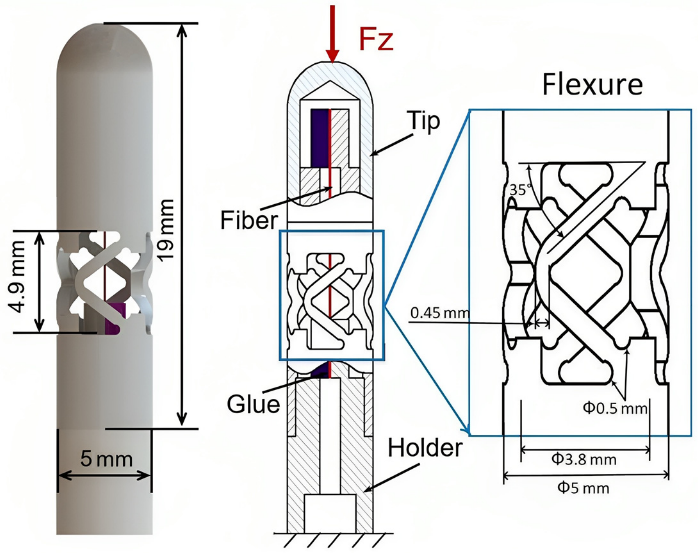

Figure 2. Designed structure (with sarrus linkage) of the proposed force sensor (adapted from [18]).

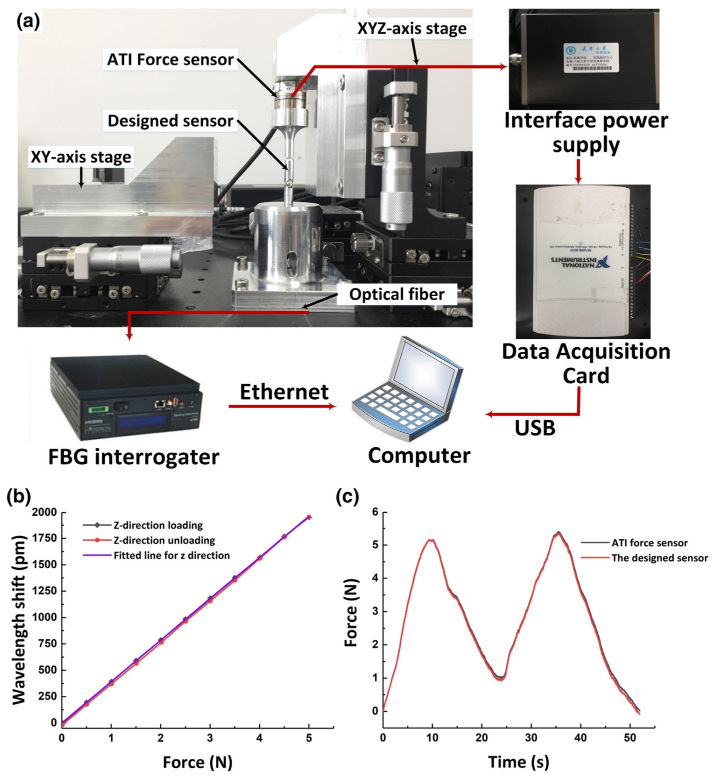

Figure 3. (**a**) Experimental configuration for force calibration of the designed sensor. (**b**) Calibration of the relationship between the exerted force and the reflective FBG central wavelength. (**c**) Comparison of force values measured from designed FBG and force/torque sensor along the Z-direction and it exhibits measured force values of FBG sensor noticeably follows commercially available torque/force sensor values, which validate the precision of the designed sensor (adapted from [18]).

As emphasized in Figure 3c, the axial sensitivity value hit 392.17 pm/N with a resolution of 2.55 mN, making it very easy to detect tissue abnormalities precisely. The axial force values measured from the prototype sensor are in tune with the commercially available T/F (torque/force) sensor. The T/F sensor was used to calibrate the prototype sensor, and the experimental data showed a linearity error of 0.97%, validating FBG's potential use for efficient force sensing in minimally invasive surgeries.

2.2. Fiber-Bragg-Grating-Instrumented Rehabilitation

The potential applications of FBG technology in rehabilitation encompass a wide range of functions. These include strain detection in bones, monitoring of bone cement, measurement of contact forces, and pressure mapping in orthopedic joints. Additionally, FBG technology can be utilized for assessing pressure distribution in intervertebral discs, monitoring chest wall deformation, and measuring forces within tendons and ligaments. It also aids in evaluating forces occurring at various angles between body parts during the gait cycle [26–28]. A. Bimis et al. measured induced strain during the hardening stage of self-setting calcium/phosphate bone cement using an embedded fiber Bragg grating sensor with a 1 mm grating length [29]. Two different cylindrical bone cement samples with embedded FBGs were created, and during the hardening process, an interrogator was used to record the peak wavelength with an interval of 24 h. Once the hardening process was completed, both specimens were exposed to different kinds of wet environments to gain weight while recording peak wavelengths. To assist the understanding of the FBG results, scanning electron microscopy (SEM) imaging was performed, and any change in the morphological structure of bone cements occurred at the curing step. Finally, after the hardening process, FBG sensors were used to obtain hygroscopic strains. As illustrated in Figure 4, the strain measurements show two different linear responses, which implies good adaptation and compatibility between calcium phosphate cement (CPC) and integrated FBG sensor, confirming the potential applicability of FBGs to investigate the kinetics of CPC.

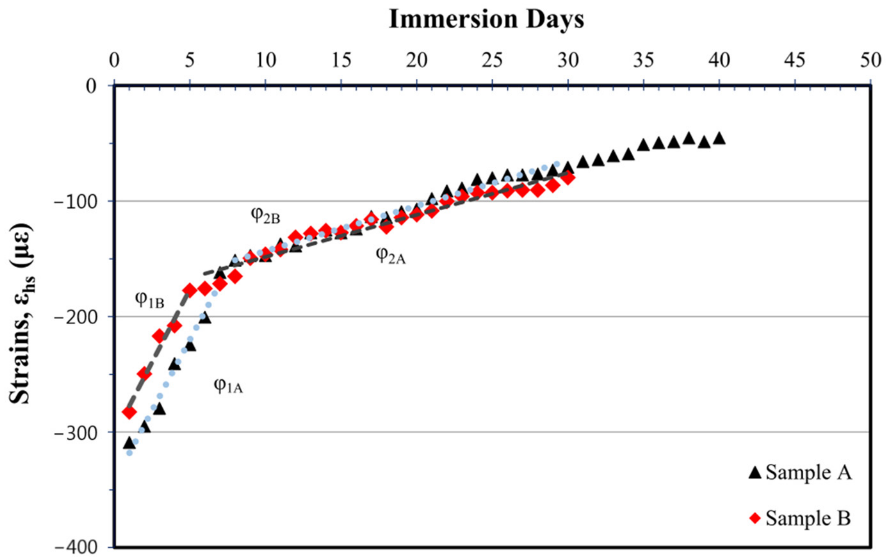

Figure 4. Induced strain during the hardening stage of 2 CPC specimens, namely Sample A and Sample B, revealed comparatively large compressive strains in the beginning. Over time, the strain became much smaller following two distinct linear paths of strain relief (adapted from [29]).

Ali Najafzadeh et al. investigated the efficacious layout of FBG with respect to the fracture position and implant plate for future works [30]. For the intact femur, three FBGs were placed close to the proximal, middle, and distal regions of the femur surface using adhesives, as shown in Figure 5. A greenstick fracture of 30° was introduced in the femur in another experiment and fixed using a three-hole implant bone plate. Figure 6 illustrates a plated femur with three FBG sensors attached at different locations longitudinally close to the fracture. Two more FBG sensors were glued to each end of the femur to compare the fractured femur with the intact one.

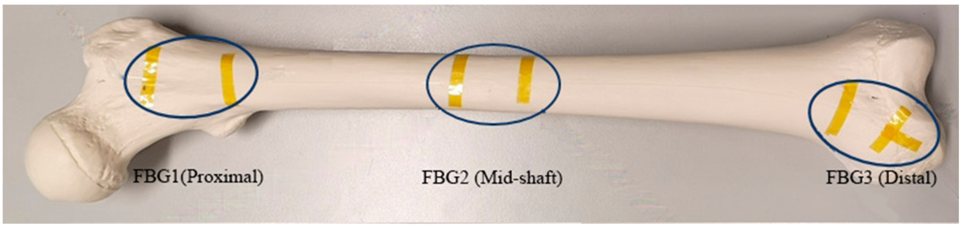

Figure 5. Intact femur with three longitudinal FBGs attached at proximal, distal, and middle regions of the femur using adhesives to measure strains (adapted from [30]).

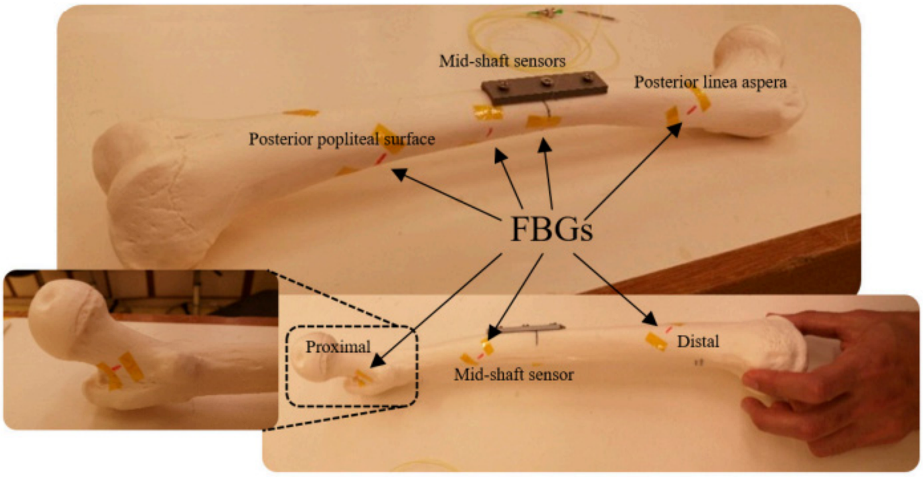

Figure 6. Plated femur with a greenstick fracture of 30° and fixed using implant bone plate. The figure shows the total of 5 longitudinal FBGs attached to the fractured femur and a total of 7 coiled FBGs employed in the final test to measure strains (adapted from [30]).

In the final test, a coiled FBG array with five and seven gratings was attached to the intact and fractured femur, respectively. For all the tests, a compression loading of under 300 N was applied to both femurs and bone strain was recorded for the femoral cortex and implant plate, as shown in Figures 7 and 8. The sensor showed a precise linear response over various loads. The higher sensitivity and the compact size of FBGs compared to the conventional strain gauges made it simpler to measure bone strains than conventional strain sensors, suggesting the successful implementation of FBGs for monitoring strain in bone.

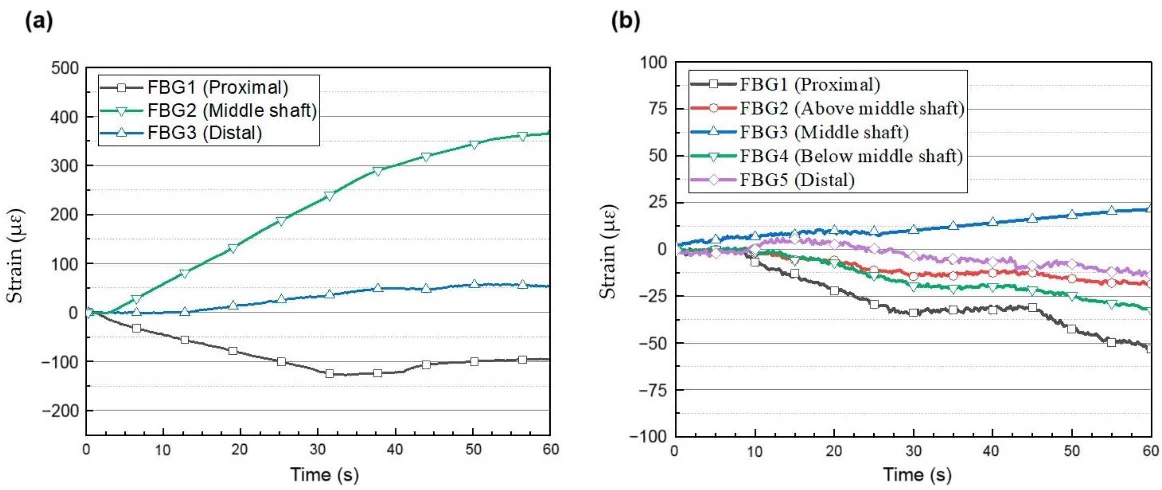

Figure 7. The subfigures show the FBGs' responses to different loadings of the intact femur: (**a**) strain values measured using longitudinal FBG arrays on the intact femur and (**b**) strain values measured using coiled FBG arrays on the intact femur (adapted from [30]).

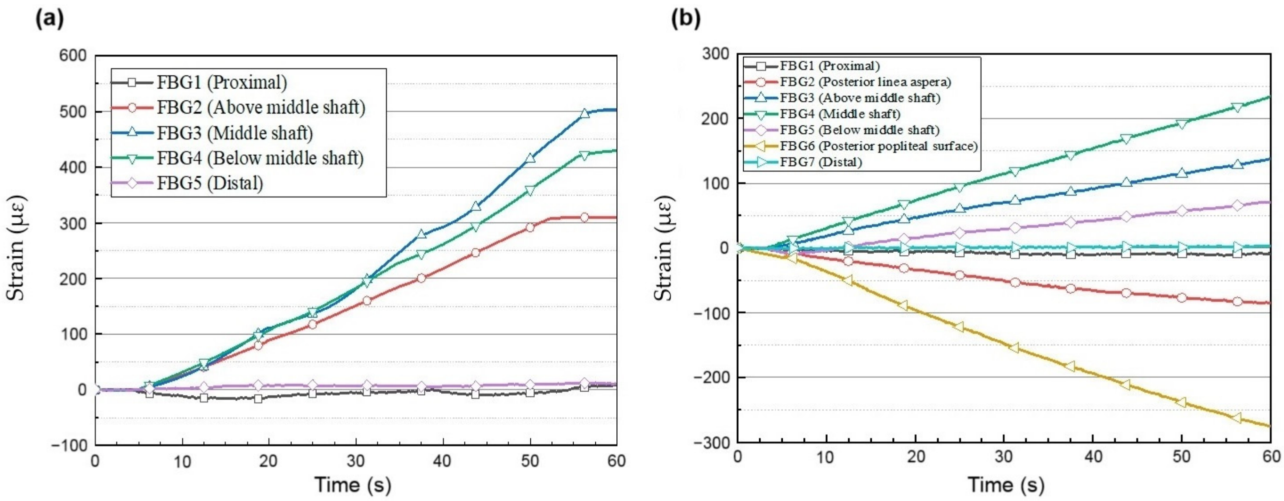

Figure 8. The subfigures show the FBGs' responses to different loadings of the plated femur: (**a**) strain values measured using longitudinal FBG arrays on the plated femur and (**b**) strain values measured using coiled FBG arrays on the plated femur (adapted from [30]).

2.3. Fiber Bragg Gratings for Prostheses

The prosthesis is a manmade device that is used to replace missing body parts or make a body part work better. With rapidly increasing amputation incidences, the need for research and development in prostheses has become critical [31,32]. To introduce the adoption of FBGs in prostheses, José Rodolfo Galvão et al. proposed a strain mapping of carbon-fiber-reinforced polymer (CFRP) lower-leg prostheses at different positions using FBG sensors [33]. After the development of a CFRP below-knee prosthesis using 65 layers of both bidirectional and unidirectional carbon-fiber fabric, eight FBG sensors were embedded in the last five layers and placed in a row perpendicular to the stress applied to monitor different stress points along the CFRP. To test the prosthesis, a candidate with a body weight of 90 kg attached the prosthesis and walked at a speed of 0.5 m/s. A comparison between the stress distribution of a loaded and unloaded prosthesis was conducted. FBGs displayed different strain responses according to their positioning in the prosthesis. For example, FBGs located at the distal end showed a weaker strain value in comparison. The experiment showed the applicability and effectiveness of FBGs in measuring strain in the below-knee prosthesis [33].

3. Force-Myography-Based Sensors

In the domain of sensors based on FMG, obtaining accurate data about limb position, orientation, and motion is crucial. This data plays a pivotal role in analyzing physical activities and advancing human–machine interface technologies, as emphasized in Reference [34]. Such information can be accomplished using optical tracking like camera technologies or wearable approaches to monitor limb movements. Comprehensive information, such as posture and applied forces, can be obtained using wearable approaches, which depend on FMG and have drawn the attention of researchers over the past couple of decades [35–37]. Creating FMG sensors involves developing force transducers to register the signals in their analog form and then converting these signals into digital form for further processing [34]. FMG is a non-invasive technique that is used to track functional movements and the position of the limb. It detects variations in the radial pressure and stiffness caused by muscle movements by placing FMG sensors (force transducers) on the selected positions with a default force [34,38].

3.1. Measuring Muscular Contraction

Alok Prakash et al. extracted information about muscle contraction using a novel dual-channel FMG sensor using a force-sensitive resistor (FSR) with high accuracy for controlling the hand prosthesis [39]. The sensor incorporates three main components: an FSR, an elastomer coupler made of polydimethylsiloxane (PDMS), and a printed assembly made of polylactic acid (PLA). The FSR is liable for uniform transmission of force across the FRS's sensing portion and gives output according to the volumetric change in muscle. To ensure consistent output from the FSR, elastomers are employed to evenly distribute muscular contractile forces across the sensing area. To prevent undesired bending and ensure even force distribution across the sensing area, the firm PLA base offers essential back support for the FSR plate. For the output analysis, FMG sensor measurement and electromyography (EMG) signals from the flexor muscles of eight subjects were simultaneously acquired using a data acquisition (DAQ) device at a sampling frequency of 2 kHz, and a two-tailed paired *t*-test was performed to compare the similarity between these two signals. The FMG sensor performed faster real-time control of a prosthetic hand in comparison to the traditional EMG sensor, with successful testing on five subjects.

3.2. FMGs in Posture Detection

In work by Eric Fujiwara et al., an FMG sensor based on the micro bending effect was used to assess muscular activities related to five hand postures for four human subjects [40]. The FMG sensor used consists of a pair of polyvinyl chloride (PVC) plates, where both plates enclose graphite rods, which are placed in a periodic arrangement with 10 mm periodicity. The upper deformer plate is attached to a silica multi-mode fiber (MMF) with light-emitting diodes (LEDs). A sufficient bending in the MMF will induce a change in the optical intensity of modulated light facilitated by the corrugated transducer. This change can be measured using a charge-coupled device (CCD) camera and processed in MATLAB. Three FMG sensors, which were placed on the subject's forearm, were used to detect the variations in forearm movements by monitoring the extensor digitorum communis (EDC), the flexor digitorum profundus (FDP), and the abductor/extensor pollicis (AEP) muscles. The system was designed to identify five postures. Artificial neural networks (ANNs) were employed to link postures with intensity signals in this study. A virtual manipulator was used to validate the applicability of the developed FMG sensor in the control of a prosthetic hand. The results confirm that virtual manipulator responses are by the FMG sensor commands in real time, which implies good adaptation of developed FMG sensors to detect hand postures with higher accuracy. Furthermore, employing a multimodal human–robot interaction (HRI) strategy can improve both the resilience and authenticity of prosthetic hand manipulation [41].

3.3. Force Myography Sensors in Human–Robot Interaction

A collision monitoring system was developed by Mohammad Anvaripour et al. using FMG of the hand of a worker and robot's dynamic parameters with the aid of eight FMG sensors [42]. Deep neural networks (DNNs) were incorporated to ensure a reliable human–robot interaction with no unnecessary collision during the work in the industry. The FMG sensors are based on force-sensing resistors (FSRs) planted to a band, which can be worn on a human hand to detect signals induced by muscle movements during interactions with the robot. In addition to that, robot dynamic parameters were also detected to find the human–robot interactions separately. By combining both the detected signals using a deep network, the researchers have been able to accurately classify between intended and unintended collisions and, based on that, a valid decision made to ensure a safe human–robot interaction. The overall results exhibit an impressive accuracy of 90% with an average detection delay of 0.2 s for this method, which validates the efficacy of the proposed method in collision monitoring during human–robot interaction.

4. Polymer Optical Fiber Sensors

Numerous important fields, such as industrial [43], medical [44], security [45], health monitoring, and physical parameter detection applications [46], use optical fiber-based sensing systems [47]. Silica and polymer optical fibers are the two major types of optical fibers (POFs) [48]. Recently, a much simpler manufacturing process, compared to conventional and other 3D printing techniques, was introduced for POF sensors. It uses 3D printing to create POF sensors. It involves adding thermochromic powders to a resin, resulting in fibers that change color when heated or cooled. These fibers are evaluated for their properties and can be used as cost-effective temperature sensors [49]. The material characteristics of POF sensors, such as high elastic strain limits, fracture toughness, high flexibility in bend, lower Young's modulus (facilitating high sensitivity for mechanical parameters), impact resistance, and relatively low cost, provide additional benefits. Owing to these benefits, several POF-sensor-based applications have been presented in this section.

4.1. Polymer Optical Fiber Sensors in Rehabilitation

The creation of a POF strain gauge based on light coupling for lower limb rehabilitation was conducted by Arnaldo G. et al. [50]. The system comprises POF strain gauges (POF-SGs), namely "illuminated" and "non-illuminated", in which the alignment difference between two POFs causes power attenuation when there is a deflection. Following the first characterization experiment, which was conducted to characterize the sensor behavior, two POF-SGs were used on a knee orthosis with a knee rehabilitation device called advanced lower-limb orthosis for rehabilitation (ALLOR) for flexion and extension exercises of knee rehabilitation (Figure 9). The flexion–extension movement is assisted by ALLOR, which consists of an admittance controller that can actively adjust the system's mechanical impedance by changing the device stiffness, damping, and inertia based on feedback from the electronic strain gauge (ESG). The degree of this assistance ranges from 1 (highest assistance) to 10 (lowest assistance) of the ALLOR, depending on the user's movement. The POF-SGs are positioned on the orthosis. Therefore, the POF-SG 2 is triggered and displays a higher power variation when the knee joint flexion movement is made. Conversely, the POF-SG 1 exhibits the greatest variance during the knee extension movement (Figure 10a). ESG is commonly used as a strain gauge in knee rehabilitation devices in robotics. In comparison with ESG, the proposed sensor showed lower variations. In the tests conducted on each of the 10 levels of assistance permitted by the controller (Figure 10b), it was validated that advantages can be provided by POF-SGs on the rehabilitation exercises and the inner controller of the rehabilitation device.

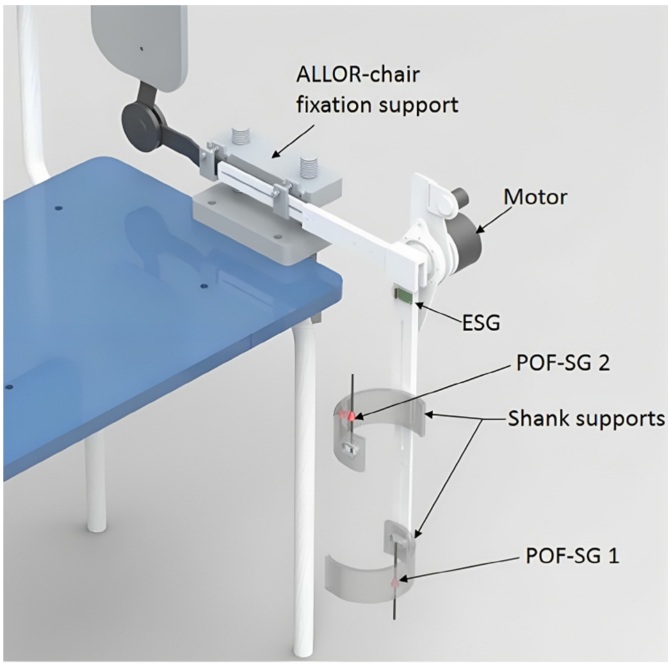

Figure 9. ESG and POF-SG positions on the ALLOR for the exercises for knee rehabilitation (adapted from [50]).

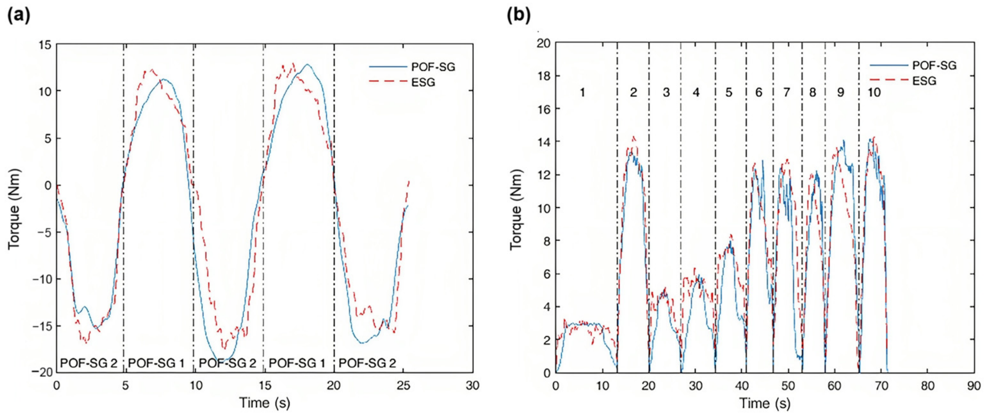

Figure 10. (**a**) Responses of POF-SGs and ESG during the knee flexion–extension workout with the impedance controller set at level 8. (**b**) Responses of POF-SGs and ESG for the knee extension exercise with the impedance controller ranging from 1 to 10 (adapted from [50]).

4.2. Polymer Optical Fiber Sensors for Gait Analysis

In-shoe plantar pressure measurements are made possible by the properties of POF. Arnaldo G. et al. presented an in-shoe measurement device for monitoring the vertical ground reaction force (GRF) during the gait cycle [51]. The system is composed of an insole comprising four POF sensors made of polymethyl methacrylate (PMMA), and sensor placements are selected based on the areas of the insole with higher plantar pressure during gait. Due to the viscoelasticity of the polymer, the polymer's response to stress or strain is not consistent. Hence, a compensating mechanism for this effect is also suggested. Sensors are connected to the light source, and each sensor has a sensitive zone that curves as it is influenced by a plantar pressure. This causes an output power variation (which can be detected using a photodiode and a transimpedance amplifier) proportionate to the curvature's angle. The presented quasistatic tests indicate the sensor's viability for measuring the vertical GRF during a gait cycle and the ability to recognize gait events throughout the stance phase.

4.3. Polymer Optical Fiber Sensors in Health Monitoring

To monitor sleep performance, Pengfei Han et al. examined the use of POF pressure sensors implanted in mattresses to evaluate respiratory and heart rate while proposing a method to increase pressure sensitivity by cutting fiber cladding and the portion of the core uniformly at 10 cm intervals [52]. The system can be broken down into three components: data processing, circuit design, and optical fiber mattress design (Figure 11).

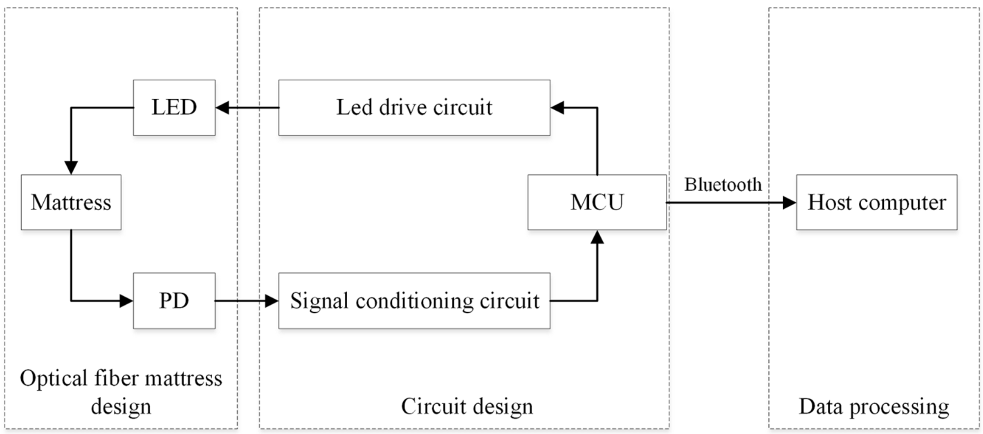

Figure 11. System structure block diagram. The voltage change results from variations in light intensity in the optical fiber delivered through the fiber bends and deformation under the pressure of the body sent to the host computer for data processing (adapted from [52]).

For sleep assessments, behavioral monitoring participants were asked to stay in four different stages, and the highest points of the energy spectrum were measured every 30 s (Figure 12). Another experiment proposed placing fibers on the second, fifth, and seventh ribs to confirm the impact of various positions on the mattress while the participant was constantly lying on his or her back, and each position's data was gathered for 30 s. The third test required participants to lie on the mattress in one of four positions, supine, left, right, or prone, to determine the impact of various sleeping postures on the sensor, and each posture's data was gathered for 30 s (Figure 13). Results show that the maximum relative errors are 6.7% and 2.4% for breathing rate and heart rate, respectively, which implies a good adaptation of the developed system for sleep performance monitoring with different sleeping postures with higher accuracy.

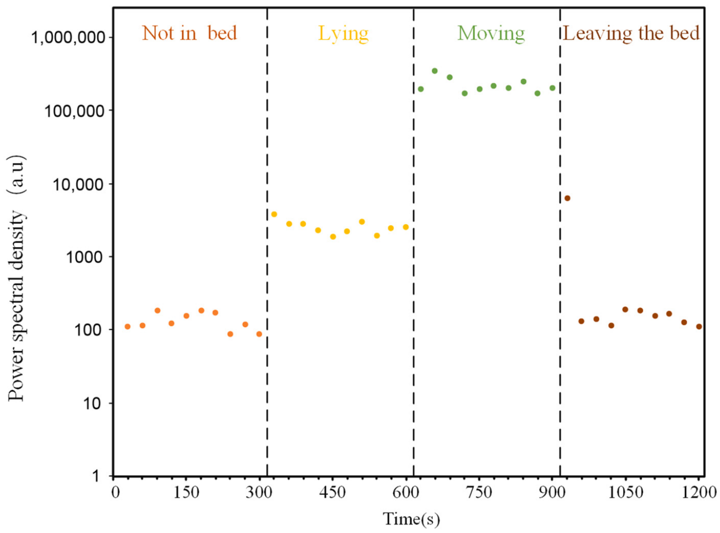

Figure 12. Power spectral density of four behavioral stages for sleep monitoring. The spectral energy is minimal when not in bed. The energy increases when lying still on the mattress, primarily by breathing and heartbeat. Slightly higher spectral energy compared to just lying when a person moves in bed. The spectral energy rapidly diminishes as they depart the mattress (adapted from [52]).

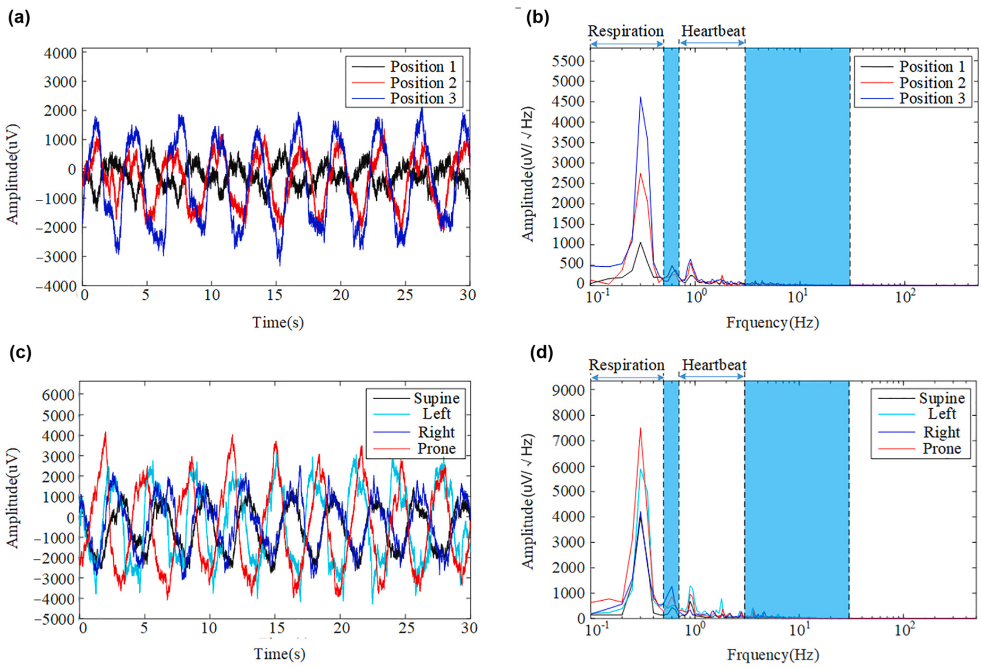

Figure 13. (**a**,**b**) Time series and power spectral density of different positions; the data from Positions 2 and 3 are more evident because they are closer to the heart. Since Position 1 is further from the heart,

there are fewer heart rate signals in this situation. Positions 1, 2, and 3 have breathing rate and heart rate measurements that are somewhat near normal ranges. (**c**,**d**) Time series and power spectral density of different postures; in any posture, the respiratory signal is obvious. Due to the asymmetry of the heart's placement within the human body, the right-side laying position produced the weakest heartbeat signal performance, while the supine and left postures demonstrated a more pronounced heartbeat signal performance (adapted from [52]).

5. Optical Tactile Sensors

The field of tactile sensor technologies includes capacitive sensors [53], piezoelectric sensors [54], piezoresistive sensors [55], quantum tunneling composites [56], and optical sensors [57,58]. These sensors come in all sizes and shapes, while some are commercially available and have been used for robotic manipulations. Their technologies have a diverse range and can be based on task-dependent designs [59]. The creation of Optical Tactile sensors involves complex steps, including microstructured surfaces, photodetectors, and precise calibration. These sensors are critical for precise tactile feedback in robotics, medical devices, and industry. Ongoing research is driving improvements in their accuracy and versatility [60].

5.1. Tissue Distinction and Discontinuity Detection in Minimally Invasive Surgeries

Robot-assisted minimally invasive surgery (RAMIS) is opening a new horizon for healthcare providers seeking a reliable solution for remote surgeries, but losing the sense of touch is a major shortcoming in RAMIS [61–65]. Due to the lack of haptic and tactile feedback, haptic feedback systems were introduced as a part of RAMIS units by Naghmeh M. Bandari et al. [66]. In this account, A hybrid force sensor was designed, modeled, simulated, fabricated, and experimentally verified to address the common problem of accurate force measurement in RAMIS applications. The sensor was fabricated using micromachining technology, whereby a V-groove, which serves as a foundation for integrating optical fibers, was bulk micromachined on the bottom surface of the beam via an anisotropic wet etching process.

Naghmeh M. Bandari proposed a hybrid force sensor, which uses the sensing principle of piezoresistivity to estimate the deformation in the tissue and directly measure the contact force and intensity modulation in optical fibers (Figure 14a). The force sensor incorporates two piezoresistive force sensing elements, eight silicon structural elements, and two separate optical fibers. Each piezoresistive element consists of two copper shell electrodes and a piezoresistive film. When one of the optical fibers was connected to a light source, the other was connected to a photodetector [67]. The schematic of the three-dimensional (3D) hybrid force sensor is shown in Figure 14b. The basic sensing concept behind this design was to measure the loss of gap power by comparing the input power (Pi) of the first fiber with the output power (Po) of the second fiber (Figure 14c).

Figure 15 illustrates the schematic experimental system, depicting the entire proposed system along with its DAQ. The lower jig of the testing machine was secured and equipped with a force sensor, while the upper jig was movable and featured a displacement sensor.

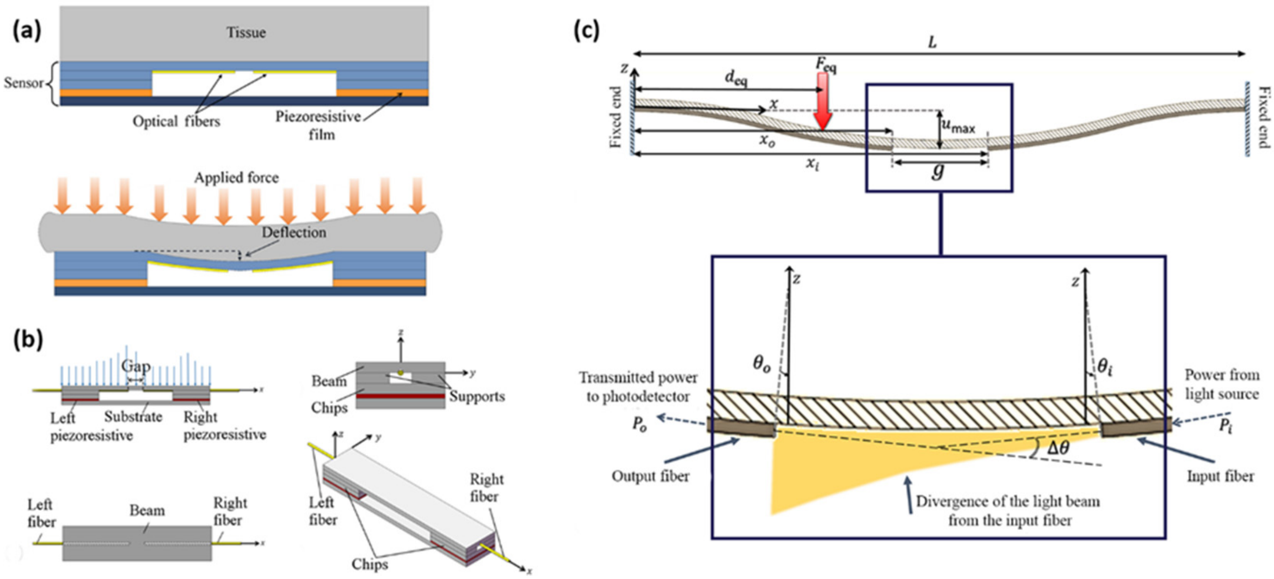

Figure 14. The schematic of the tissue and sensor with and without contact load applied from the gripping surgical tool. (**a**) Schematic of tissue and sensor with/without load from the surgical tool. (**b**) Structural design of hybrid sensor in lateral, top, longitudinal, and perspective views. (**c**) Schematic of de-formed sensor beams and detailed view of the gap between optical fibers and angular misalignment formation (adapted from [66]).

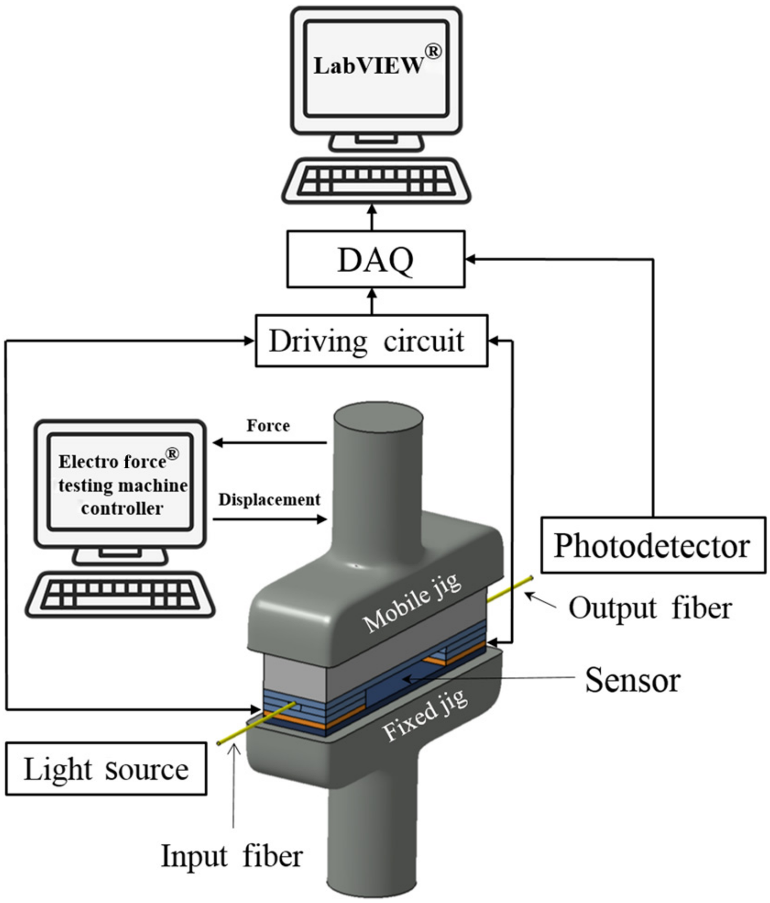

Figure 15. The experimental setup for cyclic compression is depicted (adapted from [66]).

To validate the simulations, a series of experiments were conducted under identical conditions. Figure 16a compares the estimated changes in voltage output of the photodetector obtained through finite element analysis (FEA) with the measured voltage changes from experiments in simulation. Figure 16b illustrates measured changes in voltage from actual experiments conducted using the proposed sensor for three different tissue phantoms. The force ratio variation with respect to the location of the mass is shown in Figure 16c. Figure 16d illustrates a hidden mass in motion towards a piezoresistive film, causing a change in the force ratio. A higher ratio indicates proximity to the left film.

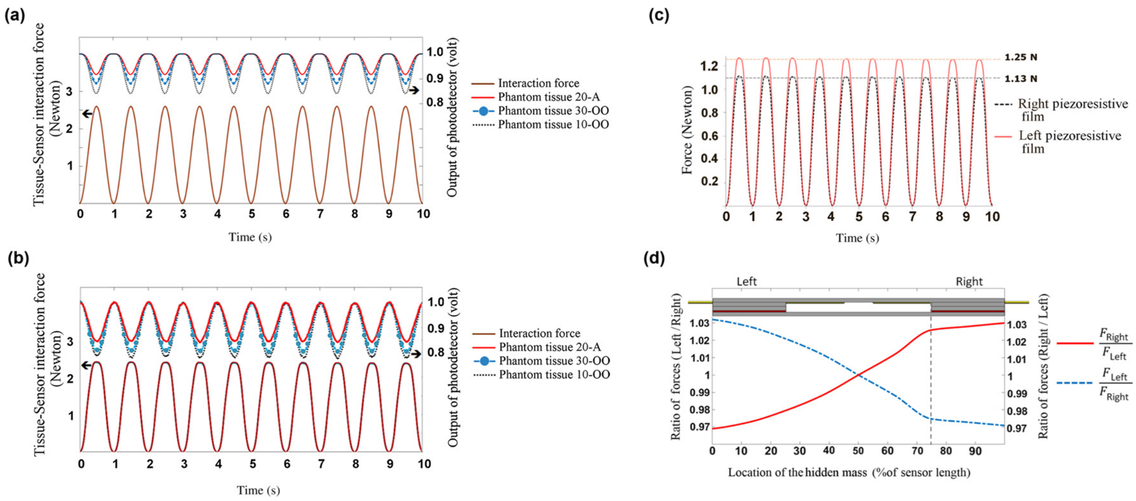

Figure 16. The estimated force between the tissue phantoms and the sensor (left axis) and the output voltage of the photodetector (right axis) obtained from the (**a**) simulation and (**b**) experiments. (**c**) Variation in the force in the left and right piezoresistive film with a hidden mass located at d = 5 mm and (**d**) variation in the ratio of forces as a function of the location of the hidden mass (adapted from [66]).

This proposed optical setup acquires data based on optical principles with the piezoresistive elements, providing a comprehensive and accurate evaluation of tissue properties and discontinuities during surgical procedures. This hybrid force sensor addresses the limitations of traditional tactile feedback in robot-assisted surgery and enhances the precision and safety of medical interventions.

5.2. Learning-Based Nonlinear Calibration for Miniaturized Optical Force Sensors

As the previous section described, loss of tactile information and lack of direct access to the internal organs are the most critical limitations of MIS, which can cause excessive or insufficient grasping force [60,68–72]. Therefore, to address this issue and improve the accuracy, dexterity, and instrument control, a simple and miniaturized optical tactile sensor to integrate MIS graspers is proposed by Naghmeh M. Bandari et al. [73]. To fabricate the sensor components, 3D printing technology was used with flexible, clear, and white resins. The sensor consists of a flexible shell fixed at both ends on a substrate. The shell had a small semi-circular indenter at the midspan of its bottom surface with a radius of 0.5 mm. A single-mode optical fiber was passed through the two substrates under the indenter and fixed (glued) to the substrate at both ends. One end of the optical fiber was connected to a light source with constant power, while the other end of the fiber was coupled to a photodetector to capture the transmitted power. Previous research studies have explored bending power loss in an optical fiber using the analytical frameworks postulated in the literature [74–78]. It was assumed that the fiber undergoes a constant bending radius (CBR) deformation. However, the CBR requirement has limited the scale of miniaturization. To address this, a variable bending radius (VBR) principle was introduced, allowing for further miniaturization. As suggested in [79], the calculated mean absolute error (MAE) has obtained excellent accuracy while meeting the requirements for reliable force measurements in MIS applications. The rate-dependent calibration has effectively captured and compensated for the hysteresis, leading to accurate results. The standard deviation of peak force for repeatability and the average difference between consecutive force estimations for resolution also met the requirements for tactile sensors in MIS applications [66,80,81].

6. Fabry–Perot Interferometry Fiber Sensor

Optical-sensor-based FPIs have been extensively studied because of their tunability and the potential to amplify signals through resonance. In recent years, FPI sensors have gained recognition as highly promising optical fiber sensors. They are preferred for their accuracy, simplicity, adaptability, responsiveness, and ability to work well in noisy environments. Fabrication of Fabry–Perot interferometry fiber sensors is a complex process involving precise etching, gap formation, and protective coating. Ongoing research aims to improve their manufacturing techniques for greater accuracy and versatility. These sensors operate by measuring the interference of light waves between two mirrors, one of which is partially transparent. By adjusting the distance between the mirrors, the sensor can be tuned to a specific wavelength, allowing for precise measurement of physical parameters such as strain, temperature, and pressure. Due to their high sensitivity and accuracy, FP interferometric sensors have been used in a wide range of applications, including structural health monitoring, industrial process control, and biomedical research [82]. Despite their advantages, the commercial growth of FPI sensors has been limited by difficulties in device fabrication. These sensors are typically fabricated using air–glass reflectors, in-fiber Bragg gratings, or semi-reflective splices.

The Bragg grating structure is created within the core of an optical fiber made of germanosilicate by utilizing an Arion laser to induce a periodic change in the refractive index [83]. Optical fiber sensors are being widely developed due to their numerous advantages over conventional sensors. These advantages include the ability to operate effectively in harsh or hostile environments, high sensitivity to various physical and chemical parameters, resistance to electromagnetic interference, and potential for multiplexing. As a result, optical fiber sensors are being used in a wide range of applications, including structural health monitoring, environmental monitoring, medical diagnostics, industrial process control, etc. [84]. Recently, there has been a significant focus on embedding optical fiber sensors into composite materials to measure strain, temperature, and vibration in various structures such as spacecraft and airplane wings. This is due to the many advantages of optical fiber sensors, such as their ability to withstand harsh environments, high sensitivity, and resistance to electromagnetic interference.

There are two broad types of FPI fiber sensors: intrinsic and extrinsic. Intrinsic sensors use an optical fiber itself as the sensing element, while extrinsic sensors use a separate structure to measure physical parameters. Recent developments in all types of FPI fiber sensors have led to significant advancements in their performance and capabilities. FPI optical fiber sensors have been utilized in numerous applications across various fields. They have been used for aircraft jet engine monitoring, where inflammable materials and high voltage electricity exist, as well as for smart structure monitoring, seismic and sonar applications, the oil industry, downhole measurement in oil wells, fiber optic gyroscopes for navigation purposes, acquiring information from small complex structures, biomechanics and rehabilitation engineering, and biological and chemical sensing. Despite the challenges in fabrication, the potential of FPI fiber sensors continues to drive research and development in this field [85].

Moreover, interferometer-based fiber-optic sensors have been utilized in various applications since the 1980s. These sensors can measure physical parameters by detecting changes in the interference pattern of light that travels through an optical fiber. As a result, interferometer-based fiber-optic sensors have been implemented in diverse fields such as aerospace, civil engineering, and biomedical research, among others. Optical coherence tomography (OCT) is an alternative method, which is mainly operated based on fiber optics and mechatronics [86–91]. This emerging opto-mechatronics technology is analogous to ultrasound imaging, except that it uses light instead of sound. Moreover, OCT can provide cross-sectional images of tissue structure on the micron scale in situ and in real time. Therefore, OCT has been extensively applied for medical, agricultural, and industrial applications [86,92–100].

6.1. FPI Sensor Fabrication Methods Using Fabry–Perot Interferometers

Several varieties of optical fibers have been used for the development of FPI sensors. Yoshino et al. fabricated an FPI sensor using single-mode fiber (SMF) by optically polishing and coating the two end faces with a multilayer of dielectric films. The single two-core fiber was employed to develop Fabry–Perot interferometric sensors for concurrent comprehensive measurement of temperature and strain. This FPI is made up of a pair of low-reflection Bragg gratings that are holographically written with a time-division multiplexing (TDM) technique. Various interesting and challenging FPI fabrication methods can be found in the literature [85,101–103].

6.2. Sensing Applications of Fabry–Perot Interferometers

FPIs excel in temperature sensing, mechanical vibration detection, acoustic wave sensing, ultrasound imaging, voltage monitoring, magnetic field measurement, pressure sensing, strain measurement, flow velocity monitoring, humidity sensing, gas detection, and liquid level sensing. The precision and sensitivity of FPIs make them essential in modern technology and research, playing a vital role in advancing various fields.

6.3. Phantom Study of a Fiber Optic Force Sensor Design for Biopsy Needles under Magnetic Resonance Imaging

One of the major problems in a biopsy operation is needle deflection during insertion. The needle deflection can be detected immediately through sudden fluctuations in continuous force measurement if a biopsy needle has an embedded force sensor. Fiber optic force sensors can be used under magnetic resonance imaging (MRI) without causing any danger or disruption to the MR image. Applied axial force measurement during needle guidance can be performed by FPI-based fiber optic force sensors, which can be integrated into the biopsy needle tip [104–107].

6.4. In-fiber Fabry–Perot Interferometer for Strain and Magnetic Field Sensing

Greice et al. conducted a comprehensive study on FPIs, which primarily focused on the application of FPIs in strain sensing, with a particular focus on scenarios where temperature variations can potentially impact the accuracy of strain measurements [108]. Researchers used a Fujikura FSM-30S fusion splicer to create cylindrical air cavities by splicing short sections (25–650 μm) of capillary fiber between standard SMF. The splicing procedure involved attaching a long section of the capillary fiber to a single-mode fiber, cleaving the capillary fiber under an optical microscope to achieve the desired air-cavity length, and then splicing the cleaved side of the capillary fiber to another single-mode fiber. Typical images of air cavities were shown, with lengths of 25 μm (Figure 17a) and 200 μm (Figure 17b). The paper also explores the use of in-fiber FPIs in magnetic field sensing. Two configurations were proposed for magnetic field sensors based on in-fiber FPIs. The first configuration involved attaching the FPI to a magnetostrictive material, and the second configuration involved placing the FPI inside a small magnet.

The researchers explore the capabilities of FPIs based on capillary optical fibers, comparing them with FBGs. The team conducted experiments to measure the temperature and strain sensitivity of FPI sensors with different air-cavity lengths. The study reveals that FPIs offer lower sensitivity to temperature changes, as their wavelength shift is directly proportional to the thermal expansion coefficient, observing temperature sensitivities in the range of 0.8 pm/°C to 1.1 pm/°C, whereas the sensitivity of FBG was ~12 pm/°C (Figure 18a). Additionally, the FPIs (air-cavity length of approximately 25μm) demonstrated remarkable strain sensitivity, with a response approximately 9.5 times higher than that of FBGs (Figure 18b).

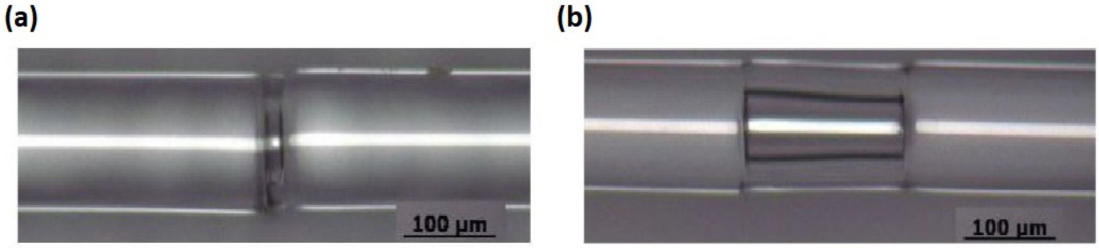

Figure 17. Air-cavities of length of (**a**) 25 µm and (**b**) 200 µm (microscope image) (adapted from [108]).

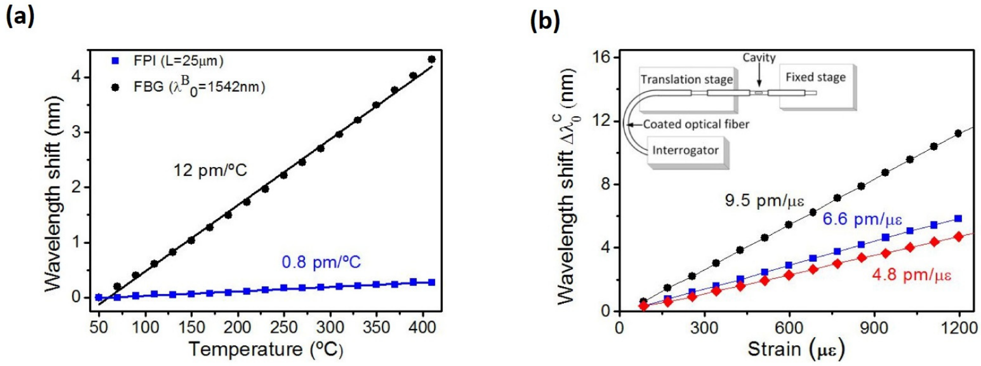

Figure 18. (**a**) The relationship between wavelength shift and temperature is examined for an FPI with an air-cavity length of L = 25 µm (λ_0) and a standard FBG ($\Delta\lambda_\beta$) (**b**) The impact of longitudinal strain on the in-fiber FPI is investigated by analyzing the wavelength shift (λ_0) in response to applied strain. The air-cavities' lengths are set at 25 µm, 55 µm, and 150 µm (adapted from [108]).

The proposed two configurations for magnetic field sensors using FPIs, each proving highly sensitive and outperforming FBG-based counterparts. One configuration involved attaching the FPI to a magnetostrictive material, achieving a sensitivity of 44 pm/mT. The second device, a magnetic force sensor, attained a calibration of 1.82 nm/N, demonstrating superior sensitivity compared to FBG-based sensors. These findings underscore the versatility of FPI sensors in addressing some unique demands of bio-mechatronics applications, where temperatures often challenge the precision and accuracy of optical sensors. Table 2 provides an overall table of the reviewed techniques, comparing each sensor.

Table 2. Fiber-optic sensors for bio-mechatronics applications.

Fiber-Optic Sensor Type	Key Features	Limitations	Typical Applications	References
FBG	High sensitivity, compact design	High cost, design complexity	Strain detection, prosthetics	[14–33]
FMG	Accurate limb movement monitoring	Requires further wearable development	Rehabilitation, human–robot interaction	[34–40,42]
POF	High elastic strain limits, flexibility	Material attenuation, biocompatibility	Gait analysis, sleep monitoring	[43–48,50–52]
Optical Tactile Sensor	Improved resolution and sensitivity	Limited hospital adoption	Robotics-assisted minimally invasive surgery	[57–59,61–66]
FPI	Measures various physical parameters	Further development is needed for prosthetic limbs	Biomedical applications, real-time monitoring	[82,83,85–90,92–95,101–108]

7. Conclusions and Future Perspectives

In the coming years, the field of bio-mechatronics is expected to experience significant growth and advancement, largely driven by the integration of advanced sensors and technological innovations. This study has explored the potential of various optical sensors, such as FBGs, FMG sensors, POFs, optical tactile sensors, and FPI fiber sensors, in enhancing bio-mechatronic applications. FBG technology has already demonstrated its potential in various bio-mechatronic applications, including the detection of strains in bones, monitoring of bone cement hardening, and measurement of contact forces in orthopedic joints. The compact nature and the high sensitivity of FBGs make them an attractive option for future strain mapping in prosthetics. Further research and development in this area have the potential to significantly improve the functionality of prosthetic devices. Similarly, the advancements in FMG technology hold tremendous promise for the future of bio-mechatronics. The use of FMG sensors in conjunction with deep neural networks has already shown the ability to accurately monitor limb movements and posture, leading to the potential for safer human–robot interactions. Moreover, the exploration of wearable FMG sensors may lead to the creation of even more advanced human–machine interface technologies. Further, POF technology has already demonstrated its potential for use in bio-mechatronic applications since POF sensors have several advantages over traditional sensors, such as their high elastic strain limits, exceptional flexibility, and impact resistance, which make them an attractive option for a wide range of applications, including rehabilitation, gait analysis, and sleep performance monitoring. Thus, future developments of POFs are focused on improving accuracy and sensitivity while enabling user-friendliness. Optical tactile sensors have undergone significant advancements over the years, which have improved their resolution and sensitivity. While these sensors have not yet been widely adopted in hospitals, their potential benefits make them a promising technology for RAMIS. Another promising direction is the integration of algorithms to enable real-time guidance and feedback during surgery. Such feedback and guidance systems can improve the accuracy and safety of RAMIS by reducing the risk of tissue damage and improving surgical outcomes.

Furthermore, the development of FPI sensors has shown remarkable progress over the years. With the ability to measure various physical parameters, such as pressure and strain, FPI sensors have become a crucial part of many biomedical applications. However, the field of FPI sensors still has much room for advancement. Future research will likely focus on developing more sensitive and precise sensors that can be integrated with other technologies to provide greater accuracy and control for real-time monitoring of physical parameters. The current studies demonstrated the feasibility of integrating a custom-designed FPI force sensor into a biopsy needle for real-time force monitoring during needle insertion and showed that the sensor could successfully detect small changes in applied force. In the future, FPI force sensors could be further developed and optimized for use in a variety of clinical applications, such as neurosurgery and cardiac surgery, where it is crucial to ensure that the forces exerted on tissues are within a safe range and also to provide real-time feedback on the forces exerted during surgery, enabling the surgeon to make more precise adjustments and avoid complications. Additionally, FPI sensors could also be useful in the development of prosthetic limbs, where accurate force sensing is necessary to achieve optimal functionality and user comfort.

In order to fully realize the potential of fiber-optic sensors in bio-mechatronic applications, further research and development is necessary. To expand their applicability in different surgical procedures and environments, there is a need to develop more compact and portable sensors that can be effortlessly integrated into surgical instruments. Despite the advantages, restricted spectral range, material attenuation, fragility, and biocompatibility concerns can be considered as the primary limitations of FOS. In addition to that, they can be costly, complex, and susceptible to environmental noise and crosstalk in multiplexed systems. Furthermore, rigorous clinical testing and validation are needed to demonstrate the effectiveness and reliability of these sensors in real-world surgical environments. To overcome these, it is imperative that researchers, medical device manufacturers, and surgeons engage in collaborative efforts to propel these technologies forward and to improve the design and performance of new and existing sensors and feedback systems. Ultimately, these efforts will bring about meaningful advancements and enhancements in the domain of bio-mechatronics in the upcoming years.

Author Contributions: Conceptualization, R.E.W., M.J. and J.K.; methodology, M.A.A.R. and R.E.W.; validation, R.E.W., B.N.S. and N.K.R.; formal analysis, M.A.A.R., N.S.K. and V.N.A.; investigation, M.A.A.R. and N.S.K.; resources, R.E.W. and U.W.; data curation, N.S.K.; writing—original draft preparation, N.S.K., R.E.W., M.A.A.R. and B.N.S.; writing—review and editing, N.S.K., R.E.W., N.K.R., and M.A.A.R.; visualization, N.S.K.; supervision, R.E.W. and N.K.R.; project administration, U.W., R.E.W. and N.K.R.; funding acquisition, N.K.R. and U.W. All authors have read and agreed to the published version of the manuscript.

Funding: This research was supported by the Science and Technology Human Resource Development Project, Ministry of Education, Sri Lanka, funded by the Asian Development Bank (Grant No. STHRD/CRG/R3/SJ/07) and partially funded by the University of Sri Jayewardenepura Research Grants, under the grant numbers of ASP/01/RE/ENG/2022/86.

Institutional Review Board Statement: Not applicable.

Informed Consent Statement: Not applicable.

Data Availability Statement: No data were used for the research described in the article.

Conflicts of Interest: The authors declare no conflict of interest.

References

1. Li, Z.; Yang, C.; Burdet, E. Guest Editorial An Overview of Biomedical Robotics and Bio-Mechatronics Systems and Applications. *IEEE Trans. Syst. Man Cybern. Syst.* **2016**, *46*, 869–874. [CrossRef]
2. Biomedical Requirements for Human Machine Interface towards Building a Humanoid: A Review | IEEE Conference Publication | IEEE Xplore. Available online: https://ieeexplore.ieee.org/abstract/document/9030298/ (accessed on 4 October 2022).
3. Wang, H.; Guo, J.-K.; Mo, H.; Zhou, X.; Han, Y. Fiber Optic Sensing Technology and Vision Sensing Technology for Structural Health Monitoring. *Sensors* **2023**, *23*, 4334. [CrossRef] [PubMed]
4. Lechler, K.; Frossard, B.; Whelan, L.; Langlois, D.; Müller, R.; Kristjansson, K. Motorized Biomechatronic Upper and Lower Limb Prostheses—Clinically Relevant Outcomes. *PMR* **2018**, *10*, S207–S219. [CrossRef]
5. Mak, Y.X.; Lanciano, A.; Stramigioli, S.; Abayazid, M. Development of Haptic Approaches for a Head-Controlled Soft Robotic Endoscope. In Proceedings of the 2020 8th IEEE RAS/EMBS International Conference for Biomedical Robotics and Biomechatronics (BioRob), New York, NY, USA, 29 November–1 December 2020; pp. 1216–1222.
6. Su, H.; Yang, C.; Ferrigno, G.; De Momi, E. Improved Human–Robot Collaborative Control of Redundant Robot for Teleoperated Minimally Invasive Surgery. *IEEE Robot. Autom. Lett.* **2019**, *4*, 1447–1453. [CrossRef]
7. Adaptable Robotic Platform for Gait Rehabilitation and Assistance: Design Concepts and Applications | SpringerLink. Available online: https://link.springer.com/chapter/10.1007/978-981-15-4732-4_5 (accessed on 5 October 2022).
8. D'Alvia, L.; Pittella, E.; Fioriello, F.; Maugeri, A.; Rizzuto, E.; Piuzzi, E.; Sogos, C.; Del Prete, Z. Heart Rate Monitoring under Stress Condition during Behavioral Analysis in Children with Neurodevelopmental Disorders. In Proceedings of the 2020 IEEE International Symposium on Medical Measurements and Applications (MeMeA), Bari, Italy, 1 June–1 July 2020; pp. 1–6.
9. Gibbs, P.T.; Asada, H. Wearable Conductive Fiber Sensors for Multi-Axis Human Joint Angle Measurements. *J. NeuroEng. Rehabil.* **2005**, *2*, 7. [CrossRef] [PubMed]
10. Vilela, D.; Romeo, A.; Sánchez, S. Flexible Sensors for Biomedical Technology. *Lab Chip* **2016**, *16*, 402–408. [CrossRef]
11. Luo, L.; Liu, Z. Recent Progress in Organic Field-Effect Transistor-Based Chem/Bio-Sensors. *VIEW* **2022**, *3*, 20200115. [CrossRef]
12. Zhou, Y.; Lian, H.; Li, Z.; Yin, L.; Ji, Q.; Li, K.; Qi, F.; Huang, Y. Crack Engineering Boosts the Performance of Flexible Sensors. *VIEW* **2022**, *3*, 20220025. [CrossRef]
13. Review of Femtosecond-Laser-Inscribed Fiber Bragg Gratings: Fabrication Technologies and Sensing Applications | Photonic Sensors. Available online: https://link.springer.com/article/10.1007/s13320-021-0629-2 (accessed on 13 October 2023).
14. Kang, L.-H.; Kim, D.-K.; Han, J.-H. Estimation of Dynamic Structural Displacements Using Fiber Bragg Grating Strain Sensors. *J. Sound Vib.* **2007**, *305*, 534–542. [CrossRef]
15. Tosi, D. Review and Analysis of Peak Tracking Techniques for Fiber Bragg Grating Sensors. *Sensors* **2017**, *17*, 2368. [CrossRef]
16. Tosi, D. Review of Chirped Fiber Bragg Grating (CFBG) Fiber-Optic Sensors and Their Applications. *Sensors* **2018**, *18*, 2147. [CrossRef]
17. Guo, Y.; Kong, J.; Liu, H.; Xiong, H.; Li, G.; Qin, L. A Three-Axis Force Fingertip Sensor Based on Fiber Bragg Grating. *Sens. Actuators A Phys.* **2016**, *249*, 141–148. [CrossRef]

18. Lv, C.; Wang, S.; Shi, C. A High-Precision and Miniature Fiber Bragg Grating-Based Force Sensor for Tissue Palpation During Minimally Invasive Surgery. *Ann. Biomed. Eng.* **2020**, *48*, 669–681. [CrossRef]
19. Yurkewich, D.S.; Escoto, A.; Trejos, A.L.; LeBel, M.-E.; Patel, R.V.; Naish, M.D. Low-Cost Force-Sensing Arthroscopic Tool Using Threaded Fiber Bragg Grating Sensors. In Proceedings of the 5th IEEE RAS/EMBS International Conference on Biomedical Robotics and Biomechatronics, Sao Paulo, Brazil, 12–15 August 2014; pp. 28–33.
20. Bandari, N.; Dargahi, J.; Packirisamy, M. Tactile Sensors for Minimally Invasive Surgery: A Review of the State-of-the-Art, Applications, and Perspectives. *IEEE Access* **2020**, *8*, 7682–7708. [CrossRef]
21. Konstantinova, J.; Jiang, A.; Althoefer, K.; Dasgupta, P.; Nanayakkara, T. Implementation of Tactile Sensing for Palpation in Robot-Assisted Minimally Invasive Surgery: A Review. *IEEE Sens. J.* **2014**, *14*, 2490–2501. [CrossRef]
22. Zarrin, P.S.; Escoto, A.; Xu, R.; Patel, R.V.; Naish, M.D.; Trejos, A.L. Development of an Optical Fiber-Based Sensor for Grasping and Axial Force Sensing. In Proceedings of the 2017 IEEE International Conference on Robotics and Automation (ICRA), Singapore, 29 May 2017–3 June 2017; pp. 939–944.
23. Lim, S.-C.; Lee, H.-K.; Park, J. Role of Combined Tactile and Kinesthetic Feedback in Minimally Invasive Surgery: Haptic Feedback in Minimmaly Invasive Surgery. *Int. J. Med. Robot. Comput. Assist. Surg.* **2015**, *11*, 360–374. [CrossRef]
24. Okamura, A.M. Haptics in Robot-Assisted Minimally Invasive Surgery. In *The Encyclopedia of Medical Robotics*; World Scientific: Singapore, 2018; pp. 317–339. ISBN 978-981-323-225-9.
25. Trejos, A.L.; Patel, R.V.; Naish, M.D. Force Sensing and Its Application in Minimally Invasive Surgery and Therapy: A Survey. *Proc. Inst. Mech. Eng. Part C J. Mech. Eng. Sci.* **2010**, *224*, 1435–1454. [CrossRef]
26. de Fátima Domingues, M.; Tavares, C.; Leite, T.; Alberto, N.; Leitão, C.; Marques, C.; Radwan, A.; Rocon, E.; Antunes, P.; André, P. Fiber Bragg Gratings as E-Health Enablers: An Overview for Gait Analysis Applications. In *Applications of Optical Fibers for Sensing*; IntechOpen: London, UK, 2018; ISBN 978-1-78985-352-0.
27. Rocha, R.P.; Silva, A.F.; Carmo, J.P.; Correia, J.H. FBG in PVC Foils for Monitoring the Knee Joint Movement during the Rehabilitation Process. In Proceedings of the 2011 Annual International Conference of the IEEE Engineering in Medicine and Biology Society, Boston, MA, USA, 30 August–3 September 2011; pp. 458–461.
28. Cheng-Yu, H.; Ahmed Abro, Z.; Yi-Fan, Z.; Ahmed Lakho, R. An FBG-Based Smart Wearable Ring Fabricated Using FDM for Monitoring Body Joint Motion. *J. Ind. Text.* **2021**, *50*, 1660–1673. [CrossRef]
29. Bimis, A.; Karalekas, D.; Bouropoulos, N.; Mouzakis, D.; Zaoutsos, S. Monitoring of Hardening and Hygroscopic Induced Strains in a Calcium Phosphate Bone Cement Using FBG Sensor. *J. Mech. Behav. Biomed. Mater.* **2016**, *60*, 195–202. [CrossRef]
30. Najafzadeh, A.; Serandi Gunawardena, D.; Liu, Z.; Tran, T.; Tam, H.-Y.; Fu, J.; Chen, B.K. Application of Fibre Bragg Grating Sensors in Strain Monitoring and Fracture Recovery of Human Femur Bone. *Bioengineering* **2020**, *7*, 98. [CrossRef]
31. Das, N.; Nagpal, N.; Bankura, S.S. A Review on the Advancements in the Field of Upper Limb Prosthesis. *J. Med. Eng. Technol.* **2018**, *42*, 532–545. [CrossRef]
32. Madusanka, D.G.K.; Wijayasingha, L.N.S.; Gopura, R.A.R.C.; Amarasinghe, Y.W.R.; Mann, G.K.I. A Review on Hybrid Myoelectric Control Systems for Upper Limb Prosthesis. In Proceedings of the 2015 Moratuwa Engineering Research Conference (MERCon), Moratuwa, Sri Lanka, 7–8 April 2015; pp. 136–141.
33. Galvao, J.R.; Zamarreno, C.R.; Martelli, C.; Cardozo Da Silva, J.C.; Arregui, F.J.; Matias, I.R. Strain Mapping in Carbon-Fiber Prosthesis Using Optical Fiber Sensors. *IEEE Sens. J.* **2017**, *17*, 3–4. [CrossRef]
34. Xiao, Z.G.; Menon, C. A Review of Force Myography Research and Development. *Sensors* **2019**, *19*, 4557. [CrossRef]
35. Fujiwara, E.; Wu, Y.T.; Santos, M.F.M.; Schenkel, E.A.; Suzuki, C.K. Development of an Optical Fiber FMG Sensor for the Assessment of Hand Movements and Forces. In Proceedings of the 2015 IEEE International Conference on Mechatronics (ICM), Nagoya, Japan, 6–8 March 2015; pp. 176–181.
36. Cho, E.; Chen, R.; Merhi, L.-K.; Xiao, Z.; Pousett, B.; Menon, C. Force Myography to Control Robotic Upper Extremity Prostheses: A Feasibility Study. *Front. Bioeng. Biotechnol.* **2016**, *4*, 18. [CrossRef] [PubMed]
37. Sakr, M.; Menon, C. Exploratory Evaluation of the Force Myography (FMG) Signals Usage for Admittance Control of a Linear Actuator. In Proceedings of the 2018 7th IEEE International Conference on Biomedical Robotics and Biomechatronics (Biorob), Enschede, The Netherlands, 26–29 August 2018; pp. 903–908.
38. Delva, M.L.; Lajoie, K.; Khoshnam, M.; Menon, C. Wrist-Worn Wearables Based on Force Myography: On the Significance of User Anthropometry. *BioMed. Eng. OnLine* **2020**, *19*, 46. [CrossRef] [PubMed]
39. Prakash, A.; Sharma, N.; Sharma, S. Novel Force Myography Sensor to Measure Muscle Contractions for Controlling Hand Prostheses. *Instrum. Sci. Technol.* **2020**, *48*, 43–62. [CrossRef]
40. Fujiwara, E.; Wu, Y.T.; Suzuki, C.K.; de Andrade, D.T.G.; Neto, A.R.; Rohmer, E. Optical Fiber Force Myography Sensor for Applications in Prosthetic Hand Control. In Proceedings of the 2018 IEEE 15th International Workshop on Advanced Motion Control (AMC), Tokyo, Japan, 9–11 March 2018; pp. 342–347.
41. Multimodal Human–Computer Interaction: A Survey—ScienceDirect. Available online: https://www.sciencedirect.com/science/article/abs/pii/S1077314206002335 (accessed on 13 October 2023).
42. Anvaripour, M.; Saif, M. Collision Detection for Human-Robot Interaction in an Industrial Setting Using Force Myography and a Deep Learning Approach. In Proceedings of the 2019 IEEE International Conference on Systems, Man and Cybernetics (SMC), Bari, Italy, 6–9 October 2019; pp. 2149–2154.
43. Johny, J.; Amos, S.; Prabhu, R. Optical Fibre-Based Sensors for Oil and Gas Applications. *Sensors* **2021**, *21*, 6047. [CrossRef]

44. Biomedical Application of Optical Fibre Sensors—IOPscience. Available online: https://iopscience.iop.org/article/10.1088/2040-8986/aac68d/meta (accessed on 29 September 2022).
45. In-Ground Optical Fibre Bragg Grating Pressure Switch for Security Applications. Available online: https://www.spiedigitallibrary.org/conference-proceedings-of-spie/8351/83510N/In-ground-optical-fibre-Bragg-grating-pressure-switch-for-security/10.1117/12.914446.short?SSO=1 (accessed on 29 September 2022).
46. Cennamo, N.; Zeni, L. Polymer Optical Fibers for Sensing. *Macromol. Symp.* **2020**, *389*, 1900074. [CrossRef]
47. Castrellon-Uribe, J. Optical Fiber Sensors: An Overview. In *Fiber Optic Sensors*; IntechOpen: London, UK, 2012; ISBN 978-953-307-922-6.
48. Leal-Junior, A.G.; Diaz, C.A.R.; Avellar, L.M.; Pontes, M.J.; Marques, C.; Frizera, A. Polymer Optical Fiber Sensors in Healthcare Applications: A Comprehensive Review. *Sensors* **2019**, *19*, 3156. [CrossRef]
49. Ahmed, I.; Ali, M.; Elsherif, M.; Butt, H. UV Polymerization Fabrication Method for Polymer Composite Based Optical Fiber Sensors. *Sci. Rep.* **2023**, *13*, 10823. [CrossRef]
50. Leal-Junior, A.G.; Frizera, A.; Marques, C.; Sánchez, M.R.A.; Botelho, T.R.; Segatto, M.V.; Pontes, M.J. Polymer Optical Fiber Strain Gauge for Human-Robot Interaction Forces Assessment on an Active Knee Orthosis. *Opt. Fiber Technol.* **2018**, *41*, 205–211. [CrossRef]
51. Leal-Junior, A.G.; Frizera, A.; Avellar, L.M.; Marques, C.; Pontes, M.J. Polymer Optical Fiber for In-Shoe Monitoring of Ground Reaction Forces During the Gait. *IEEE Sens. J.* **2018**, *18*, 2362–2368. [CrossRef]
52. Han, P.; Li, L.; Zhang, H.; Guan, L.; Marques, C.; Savović, S.; Ortega, B.; Min, R.; Li, X. Low-Cost Plastic Optical Fiber Sensor Embedded in Mattress for Sleep Performance Monitoring. *Opt. Fiber Technol.* **2021**, *64*, 102541. [CrossRef]
53. Muhammad, H.B.; Recchiuto, C.; Oddo, C.M.; Beccai, L.; Anthony, C.J.; Adams, M.J.; Carrozza, M.C.; Ward, M.C.L. A Capacitive Tactile Sensor Array for Surface Texture Discrimination. *Microelectron. Eng.* **2011**, *88*, 1811–1813. [CrossRef]
54. Göger, D.; Gorges, N.; Wörn, H. Tactile Sensing for an Anthropomorphic Robotic Hand: Hardware and Signal Processing. In Proceedings of the 2009 IEEE International Conference on Robotics and Automation, Kobe, Japan, 12–17 May 2009; pp. 2972–2978.
55. Stassi, S.; Cauda, V.; Canavese, G.; Pirri, C.F. Flexible Tactile Sensing Based on Piezoresistive Composites: A Review. *Sensors* **2014**, *14*, 5296–5332. [CrossRef] [PubMed]
56. Zhang, T.; Liu, H.; Jiang, L.; Fan, S.; Yang, J. Development of a Flexible 3-D Tactile Sensor System for Anthropomorphic Artificial Hand. *IEEE Sens. J.* **2013**, *13*, 510–518. [CrossRef]
57. Ward-Cherrier, B.; Pestell, N.; Cramphorn, L.; Winstone, B.; Giannaccini, M.E.; Rossiter, J.; Lepora, N.F. The TacTip Family: Soft Optical Tactile Sensors with 3D-Printed Biomimetic Morphologies. *Soft Robot.* **2018**, *5*, 216–227. [CrossRef] [PubMed]
58. Yuan, W.; Dong, S.; Adelson, E.H. GelSight: High-Resolution Robot Tactile Sensors for Estimating Geometry and Force. *Sensors* **2017**, *17*, 2762. [CrossRef]
59. Macdonald, F.L.A.; Lepora, N.F.; Conradt, J.; Ward-Cherrier, B. Neuromorphic Tactile Edge Orientation Classification in an Unsupervised Spiking Neural Network. *Sensors* **2022**, *22*, 6998. [CrossRef]
60. Othman, W.; Lai, Z.-H.A.; Abril, C.; Barajas-Gamboa, J.S.; Corcelles, R.; Kroh, M.; Qasaimeh, M.A. Tactile Sensing for Minimally Invasive Surgery: Conventional Methods and Potential Emerging Tactile Technologies. *Front. Robot. AI* **2022**, *8*, 705662. [CrossRef]
61. Leal Ghezzi, T.; Campos Corleta, O. 30 Years of Robotic Surgery. *World J. Surg.* **2016**, *40*, 2550–2557. [CrossRef] [PubMed]
62. Vyas, D.; Cronin, S. Peer Review and Surgical Innovation: Robotic Surgery and Its Hurdles. *Am. J. Robot. Surg.* **2015**, *2*, 39–44. [CrossRef]
63. Ehrampoosh, A.; Shirinzadeh, B.; Pinskier, J.; Smith, J.; Moshinsky, R.; Zhong, Y. A Force-Feedback Methodology for Teleoperated Suturing Task in Robotic-Assisted Minimally Invasive Surgery. *Sensors* **2022**, *22*, 7829. [CrossRef] [PubMed]
64. Krebs, T.F.; Schnorr, I.; Heye, P.; Häcker, F.-M. Robotically Assisted Surgery in Children—A Perspective. *Children* **2022**, *9*, 839. [CrossRef] [PubMed]
65. Lu, X.; Wang, C.; Jin, X.; Li, J. A Flexible Surgical Instrument for Robot-Assisted Minimally Invasive Surgery. *Actuators* **2022**, *11*, 206. [CrossRef]
66. Bandari, N.M.; Ahmadi, R.; Hooshiar, A.; Dargahi, J.; Packirisamy, M. Hybrid Piezoresistive-Optical Tactile Sensor for Simultaneous Measurement of Tissue Stiffness and Detection of Tissue Discontinuity in Robot-Assisted Minimally Invasive Surgery. *J. Biomed. Opt.* **2017**, *22*, 77002. [CrossRef]
67. Zhu, W.; Yang, S.; Zheng, H.; Zhan, Y.; Li, D.; Cen, G.; Tang, J.; Lu, H.; Zhang, J.; Zhao, Z.; et al. Gold Enhanced Graphene-Based Photodetector on Optical Fiber with Ultrasensitivity over Near-Infrared Bands. *Nanomaterials* **2022**, *12*, 124. [CrossRef]
68. Hortamani, R.; Zabihollah, A. Modeling and Simulation of Graspers Force in Minimally Invasive Surgery. In Proceedings of the 2009 International Association of Computer Science and Information Technology—Spring Conference, Singapore, 17–20 April 2009; pp. 475–479.
69. Abiri, A.; Pensa, J.; Tao, A.; Ma, J.; Juo, Y.-Y.; Askari, S.J.; Bisley, J.; Rosen, J.; Dutson, E.P.; Grundfest, W.S. Multi-Modal Haptic Feedback for Grip Force Reduction in Robotic Surgery. *Sci. Rep.* **2019**, *9*, 5016. [CrossRef]
70. Waters, I.; Jones, D.; Alazmani, A.; Culmer, P. Encouraging and Detecting Preferential Incipient Slip for Use in Slip Prevention in Robot-Assisted Surgery. *Sensors* **2022**, *22*, 7956. [CrossRef] [PubMed]
71. Deng, Z.; Jonetzko, Y.; Zhang, L.; Zhang, J. Grasping Force Control of Multi-Fingered Robotic Hands through Tactile Sensing for Object Stabilization. *Sensors* **2020**, *20*, 1050. [CrossRef]

72. Huang, C.; Wang, Q.; Zhao, M.; Chen, C.; Pan, S.; Yuan, M. Tactile Perception Technologies and Their Applications in Minimally Invasive Surgery: A Review. *Front. Physiol.* **2020**, *11*, 611596. [CrossRef] [PubMed]
73. Bandari, N.; Dargahi, J.; Packirisamy, M. Miniaturized Optical Force Sensor for Minimally Invasive Surgery With Learning-Based Nonlinear Calibration. *IEEE Sens. J.* **2020**, *20*, 3579–3592. [CrossRef]
74. Gauthier, R.C.; Ross, C. Theoretical and Experimental Considerations for a Single-Mode Fiber-Optic Bend-Type Sensor. *Appl. Opt.* **1997**, *36*, 6264–6273. [CrossRef]
75. Zendehnam, A.; Mirzaei, M.; Farashiani, A.; Farahani, L. Investigation of Bending Loss in a Single-Mode Optical Fibre. *Pramana-J. Phys.* **2010**, *74*, 591–603. [CrossRef]
76. Savović, S.; Djordjevich, A.; Savović, I. Theoretical Investigation of Bending Loss in Step-Index Plastic Optical Fibers. *Opt. Commun.* **2020**, *475*, 126200. [CrossRef]
77. Quiño, J.; Confesor, M. Power Loss Due to Macrobending in an Optical Fiber. In Proceedings of the 7th SPVM Physics Conference, Iligan City, Philippines, 2005.
78. Waluyo, T.; Bayuwati, D.; Mulyanto, I. The Effect of Macro-Bending on Power Confinement Factor in Single Mode Fibers. *J. Phys. Conf. Ser.* **2018**, *985*, 012001. [CrossRef]
79. Zarrin, P.S.; Escoto, A.; Xu, R.; Patel, R.V.; Naish, M.D.; Trejos, A.L. Development of a 2-DOF Sensorized Surgical Grasper for Grasping and Axial Force Measurements. *IEEE Sens. J.* **2018**, *18*, 2816–2826. [CrossRef]
80. Hooshiar, A.; Najarian, S.; Dargahi, J. Haptic Telerobotic Cardiovascular Intervention: A Review of Approaches, Methods, and Future Perspectives. *IEEE Rev. Biomed. Eng.* **2020**, *13*, 32–50. [CrossRef]
81. Ahmadi, R.; Arbatani, S.; Packirisamy, M.; Dargahi, J. Micro-Optical Force Distribution Sensing Suitable for Lump/Artery Detection. *Biomed. Microdevices* **2015**, *17*, 10. [CrossRef]
82. Etalons | LightMachinery. Available online: https://lightmachinery.com/optics/custom-optics/etalons/?gclid=CjwKCAiAl9efBhAkEiwA4TorivQ5hR3l0nhK7QTzIpbSkBXEJ6cBieX4tNCSpxTqG4QFQ7u2Zs8vhBoCFSUQAvD_BwE&gclid=CjwKCAiAl9efBhAkEiwA4TorivQ5hR3l0nhK7QTzIpbSkBXEJ6cBieX4tNCSpxTqG4QFQ7u2Zs8vhBoCFSUQAvD_BwE (accessed on 12 March 2023).
83. Ascorbe, J.; Corres, J.M.; Arregui, F.J.; Matias, I.R. Recent Developments in Fiber Optics Humidity Sensors. *Sensors* **2017**, *17*, 893. [CrossRef]
84. Pendão, C.; Silva, I. Optical Fiber Sensors and Sensing Networks: Overview of the Main Principles and Applications. *Sensors* **2022**, *22*, 7554. [CrossRef]
85. Islam, M.R.; Ali, M.M.; Lai, M.-H.; Lim, K.-S.; Ahmad, H. Chronology of Fabry-Perot Interferometer Fiber-Optic Sensors and Their Applications: A Review. *Sensors* **2014**, *14*, 7451–7488. [CrossRef]
86. Wijesinghe, R.E.; Park, K.; Kim, D.-H.; Jeon, M.; Kim, J. In Vivo Imaging of Melanoma-Implanted Magnetic Nanoparticles Using Contrast-Enhanced Magneto-Motive Optical Doppler Tomography. *J. Biomed. Opt.* **2016**, *21*, 064001. [CrossRef]
87. Fercher, A.F.; Drexler, W.; Hitzenberger, C.K.; Lasser, T. Optical Coherence Tomography—Principles and Applications. *Rep. Prog. Phys.* **2003**, *66*, 239. [CrossRef]
88. Tomlins, P.H.; Wang, R.K. Theory, Developments and Applications of Optical Coherence Tomography. *J. Phys. D Appl. Phys.* **2005**, *38*, 2519. [CrossRef]
89. Jung, W.; Kim, J.; Jeon, M.; Chaney, E.J.; Stewart, C.N.; Boppart, S.A. Handheld Optical Coherence Tomography Scanner for Primary Care Diagnostics. *IEEE Trans. Biomed. Eng.* **2011**, *58*, 741–744. [CrossRef]
90. Jeon, M.; Kim, J.; Jung, U.; Lee, C.; Jung, W.; Boppart, S.A. Full-Range k-Domain Linearization in Spectral-Domain Optical Coherence Tomography. *Appl. Opt.* **2011**, *50*, 1158–1163. [CrossRef] [PubMed]
91. Wijesinghe, R.; Lee, S.-Y.; Ravichandran, N.K.; Shirazi, M.F.; Kim, P.; Jung, H.-Y.; Jeon, M.; Kim, A. Optical Screening of Venturianashicola Caused Pyruspyrifolia (Asian Pear) Scab Using Optical Coherence Tomography. *Int. J. Appl. Eng. Res.* **2016**, *11*, 7728–7731.
92. Sensors | Free Full-Text | Overview of Fiber Optic Sensor Technologies for Strain/Temperature Sensing Applications in Composite Materials. Available online: https://www.mdpi.com/1424-8220/16/1/99 (accessed on 12 March 2023).
93. Wijesinghe, R.E.; Lee, S.-Y.; Ravichandran, N.K.; Shirazi, M.F.; Kim, P.; Jung, H.-Y.; Jeon, M.; Kim, J. Biophotonic Approach for the Characterization of Initial Bitter-Rot Progression on Apple Specimens Using Optical Coherence Tomography Assessments. *Sci. Rep.* **2018**, *8*, 15816. [CrossRef] [PubMed]
94. Saleah, S.A.; Seong, D.; Han, S.; Wijesinghe, R.E.; Ravichandran, N.K.; Jeon, M.; Kim, J. Integrated Quad-Scanner Strategy-Based Optical Coherence Tomography for the Whole-Directional Volumetric Imaging of a Sample. *Sensors* **2021**, *21*, 1305. [CrossRef]
95. Wijesinghe, R.E.; Park, K.; Jung, Y.; Kim, P.; Jeon, M.; Kim, J. Industrial Resin Inspection for Display Production Using Automated Fluid-Inspection Based on Multimodal Optical Detection Techniques. *Opt. Lasers Eng.* **2017**, *96*, 75–82. [CrossRef]
96. Ravichandran, N.K.; Wijesinghe, R.E.; Lee, S.-Y.; Choi, K.S.; Jeon, M.; Jung, H.-Y.; Kim, J. Non-Destructive Analysis of the Internal Anatomical Structures of Mosquito Specimens Using Optical Coherence Tomography. *Sensors* **2017**, *17*, 1897. [CrossRef] [PubMed]
97. Seong, D.; Han, S.; Jeon, D.; Kim, Y.; Wijesinghe, R.E.; Ravichandran, N.K.; Lee, J.; Lee, J.; Kim, P.; Lee, D.-E.; et al. Dynamic Compensation of Path Length Difference in Optical Coherence Tomography by an Automatic Temperature Control System of Optical Fiber. *IEEE Access* **2020**, *8*, 77501–77510. [CrossRef]

98. Ravichandran, N.K.; Hur, H.; Kim, H.; Hyun, S.; Bae, J.Y.; Kim, D.U.; Kim, I.J.; Nam, K.-H.; Chang, K.S.; Lee, K.-S. Label-Free Photothermal Optical Coherence Microscopy to Locate Desired Regions of Interest in Multiphoton Imaging of Volumetric Specimens. *Sci. Rep.* **2023**, *13*, 3625. [CrossRef]
99. Ravichandran, N.K.; Lakshmikantha, H.T.; Park, H.-S.; Jeon, M.; Kim, J. Micron-Scale Human Enamel Layer Characterization after Orthodontic Bracket Debonding by Intensity-Based Layer Segmentation in Optical Coherence Tomography Images. *Sci. Rep.* **2021**, *11*, 10831. [CrossRef]
100. Lee, K.-S.; Ravichandran, N.K.; Yeo, W.-J.; Hur, H.; Hyun, S.; Bae, J.Y.; Kim, D.U.; Jong Kim, I.; Nam, K.-H.; Bog, M.G.; et al. Spectrally Encoded Dual-Mode Interferometry with Orthogonal Scanning. *Opt. Express* **2023**, *31*, 10500–10511. [CrossRef]
101. Ulgen, N.O.; Uzun, D.; Kocaturk, O. Phantom Study of a Fiber Optic Force Sensor Design for Biopsy Needles under MRI. *Biomed. Opt. Express* **2018**, *10*, 242–251. [CrossRef]
102. Huang, J.; Wang, T.; Hua, L.; Fan, J.; Xiao, H.; Luo, M. A Coaxial Cable Fabry-Perot Interferometer for Sensing Applications. *Sensors* **2013**, *13*, 15252–15260. [CrossRef]
103. Gomes, A.D.; Becker, M.; Dellith, J.; Zibaii, M.I.; Latifi, H.; Rothhardt, M.; Bartelt, H.; Frazão, O. Multimode Fabry–Perot Interferometer Probe Based on Vernier Effect for Enhanced Temperature Sensing. *Sensors* **2019**, *19*, 453. [CrossRef] [PubMed]
104. Force Sensor | Measuring Force | How It Works | FUTEK. Available online: https://www.futek.com/force-sensor (accessed on 22 February 2023).
105. Lee, B.H.; Kim, Y.H.; Park, K.S.; Eom, J.B.; Kim, M.J.; Rho, B.S.; Choi, H.Y. Interferometric Fiber Optic Sensors. *Sensors* **2012**, *12*, 2467–2486. [CrossRef]
106. Arata, J.; Nitta, T.; Nakatsuka, T.; Kawabata, T.; Matsunaga, T.; Haga, Y.; Harada, K.; Mitsuishi, M. Modular Optic Force Sensor for a Surgical Device Using a Fabry–Perot Interferometer. *Appl. Sci.* **2019**, *9*, 3454. [CrossRef]
107. Gao, H.; Wang, J.; Shen, J.; Zhang, S.; Xu, D.; Zhang, Y.; Li, C. Study of the Vernier Effect Based on the Fabry–Perot Interferometer: Methodology and Application. *Photonics* **2021**, *8*, 304. [CrossRef]
108. Costa, G.; Gouvêa, P.; Soares, L.; Pereira, J.M.; Favero, F.; Braga, A.; Palffy-Muhoray, P.; Bruno, A.; Carvalho, I.C. In-Fiber Fabry-Perot Interferometer for Strain and Magnetic Field Sensing. *Opt. Express* **2016**, *24*, 14690. [CrossRef] [PubMed]